Fabrication of a Planar Optical Add/Drop Channel Filter in Silicon Oxynitride

by

Joseph C. Huang

B.S. Electrical and Computer Engineering,
Carnegie Mellon University (1999)

Submitted to the Department of Electrical Engineering and Computer Science
in partial fulfillment of the requirements for the degree of

Master of Science

at the

MASSACHUSETTS INSTITUTE OF TECHNOLOGY

May, 2002

© Massachusetts Institute of Technology, 2002. All Rights Reserved.

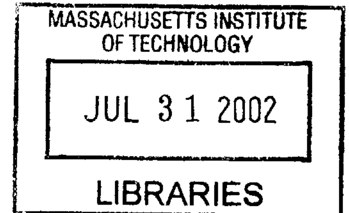

Signature of Author ....
Department of Electrical Engineering and Computer Science
May 24, 2002

Certified by ....
Henry I. Smith
Keithley Professor of Electrical Engineering
Thesis Supervisor

Accepted by ....
Arthur C. Smith
Chairman, Department Committee on Graduate Students

Fabrication of a Planar Optical Add/Drop Channel Filter in Silicon Oxynitride

by

Joseph C. Huang

Submitted to the Department of Electrical Engineering and Computer Science
in partial fulfillment of the requirements for the degree of

Master of Science

Abstract

Optical networks form the foundation of high performance local area networks (LANs) and the Internet. In order to maximize the use of the optical fiber, add/drop channel filters are needed to implement wavelength division multiplexing (WDM). The implementation of Bragg-grating-based optical devices can take advantage of planar fabrication techniques which can yield smaller, more reliable, and cheaper channel filters than what is currently used today. A new material system, silicon oxynitride, is used to solve problems from previous work involving the top cladding deposition. It also enables wide flexibility over the waveguide index contrast. Plasma enhanced chemical vapor deposition (PECVD) was used to deposit thick oxides and fill in high aspect ratio trenches by resputtering.

Thesis Supervisor: Henry I. Smith
Title: Keithley Professor of Electrical Engineering, MIT

Acknowledgments

I consider myself extremely fortunate to be able to work under the supervision of Professor Hank Smith in the NanoStructures Laboratory he created. I take away more than just knowledge. He has created an environment where all the students that work under him converse daily and think through problems together. The fostering of self-motivation and independence while still being available for questions and interaction has made life at MIT worthwhile. I have much to thank Hank for letting me work on this project.

Countless people have composed the optics group within NSL that have either left to pursue their careers or are still working diligently. This thesis would not have been possible were it not for Tom Murphy. It was his work I have based much of my thesis upon I would like to thank Michael Lim for starting me off when I first joined the group and getting my hands dirty in the lab. I appreciate my last few months with Todd Hastings who gave much valuable insight into my process as well as pleasant conversations on current state of affairs. Tymon Barwicz was a great resource with his depth of knowledge in material science. I would also like to thank Jalal Kahn for the creation of the optics test bench setup and for his deep insight into optical devices.

Jim Daley must be recognized for his dedication in making the lab run smoothly and for fulfilling my constant requests to evaporate or fix something. Thanks go to Mark Mondol who helped fix the sputter deposition system and administered to the tool formerly known as VS2A. Thanks also go to Jimmy Carter for seeing that the SEM was always up and running. If it weren't for Jessica Sandland, the Metricon would never have found its way to MIT.

I would like to thank my officemate Feng Zhang for our discussions on issues we were both having, rides to fast food joints, and for the late nights I had him using the Raith for me. Minghao Qi was invaluable for his experiences with the Plasmaquest and for his graciousness in letting me use his sleeping apparatus. Much thanks is given to Mike Walsh who put together the Lloyd's mirror. My nights were never lonely due to the presence of Tim Savas and his ever support for the Yankees. I will always remember the shared rantings on the Raith with Dario Gil and will look fondly upon the nights ridding planets of alien species with Euclid Moon and Rajesh Menon.

And finally, I would like to acknowledge my parents and my brother, Eugene, who put up with my graduate school experiences. Their love and support will never be taken for granted.

Table of Contents

1. Introduction 7

1.1 Wavelength Division Multiplexing 7

1.2 Planar Fabrication 9

1.3 Bragg Gratings 11

2. Process Overview 13

2.1 Add/Drop Channel Filter 13

2.2 Process Flow 14

2.3 Dual Layer Hard-mask 14

3. Design and Fabrication 17

3.1 Lower Cladding and Core Deposition 18

3.1.1 Dielectric Waveguides 18

3.1.2 Plasma Enhanced Chemical Vapor Deposition 20

3.1.3 Annealing 23

3.1.4 Chemical Mechanical Polishing 25

3.1.5 Measurement of Thin Films 25

3.1.6 Processing 30

3.1.7 Summary 32

3.2 Bragg Grating Hard-mask Definition 33

3.2.1 Grating Strength 33

3.2.2 Interference Lithography 37

3.2.3 Lloyd's Mirror 39

3.2.4 Measurement of Gratings 39

3.2.5 Processing 41

3.2.6 Summary 43

3.3 Waveguide Hard-mask Definition 44

3.3.1 Couplers 44

3.3.2 Bends 45

3.3.3 Waveguide Pattern Generation 47

3.3.4 Measurement of Line Profiles and Widths and Dynamic Deflection 48
3.3.5 Processing 52
3.3.6 Summary 52
3.4 Etching of Waveguides and Gratings 53
3.4.1 Waveguide Hard-mask Dry Etching 53
3.4.2 Oxynitride Dry Etching 55
3.4.3 Processing 57
3.4.4 Summary 60
3.5 Top Cladding Deposition 61
3.5.1 ECR Plasma Enhanced Chemical Vapor Deposition 61
3.5.2 Conformal Deposition 62
3.5.3 Measurement of Thin Films 65
3.5.4 Processing 66
3.5.5 Summary 67
4. Conclusion and Future Work 69
References 71

Chapter 1

Introduction

This thesis will describe the fabrication process that was implemented to produce simple waveguides and Bragg-grating-based optical devices in an embedded channel waveguide structure. Adding onto previous work done at the NanoStructures Laboratory (NSL), a new material system is introduced which provides solutions to issues regarding the final top cladding deposition. The purpose of this thesis is to provide a stepping-stone to those who will complete the fabrication of an integrated Bragg grating add/drop channel filter. Therefore, much detail will be placed in the processing steps as well as brief discussions will be given to the design steps to maximize transfer of knowledge.

The structure of this thesis will exemplify the intertwining of design and fabrication by describing the flow of thought that was used to tackle the task of fabricating these optical devices. This is in the attempt to provide a person who is new to the field of optics and fabrication techniques a shallower learning curve to understanding the nature of these devices. References are given to previous work done here at NSL and elsewhere for further insight into the theory involved in the design aspects.

The new material system employs silicon oxynitride, a mixture of silicon oxide and silicon nitride. The ability to deposit a wide range of refractive indices with stress control makes oxynitride very attractive. PECVD systems are available on the MIT campus to deposit these films enabling prototyping of optical devices without seeking outside service vendors. A dual RF plasma enhanced chemical vapor deposition (PECVD) system is used to deposit thick oxide and oxynitride layers. An electron cyclotron resonance (ECR) plasma enhanced chemical vapor deposition (PECVD) system with RF substrate bias control is utilized to fill high aspect ratio gratings via resputtering.

1.1 Wavelength Division Multiplexing

The late 1990s experienced a tremendous boom in connectivity between people across the globe as prices for personal computers plummeted, allowing the masses to affordably purchase and connect to the rapidly growing Internet. Increased use of

network backbones of internet service providers as well as demand for high speed data links to homes and offices has been the driving force for networks that can support more users, with higher speed, all for lower cost.

Fortunately, research in optical materials and lasers have provided a means to support the demands of the public as well as the fattening of wallets for corporate executives. Ever since the mid-1960s, early experiments demonstrated that information can be encoded in light and transmitted over a glass fiber waveguide. It was not until the early 1970s that low-loss optical fibers, invented by Corning Laboratories, enabled optical fiber transmission systems to be realized for long distance communications. These silica-based fibers had low loss transmission windows in the 0.8, 1.3, and 1.55um infrared wavelength bands with the lowest loss in the 1.55um band [1].

After the first optical fibers were made, research in laser technology as well as specially designed fibers have continually solved problems that stunted the full potential of optical networks in terms of the distance signals can travel, the bitrate that can be transmitted, and the reuse of old infrastructure to reduce cost. However, the full theoretical maximum throughput for optical fibers is still very hard to achieve. Also, the infrastructure costs to give each connection their own fiber is incredibly expensive. The development of wavelength division multiplexing (WDM) breathed new life into existing optical networks thanks to the development of erbium doped fiber amplifiers (EDFA).

WDM allows multiple users to simultaneously use an optical fiber by assigning each user a portion of the available transmission wavelengths. With the success of EDFA, which can amplify multiple wavelengths at once, WDM heralded a new form of optical networking, creating virtual fibers while maximizing the use of existing infrastructure.

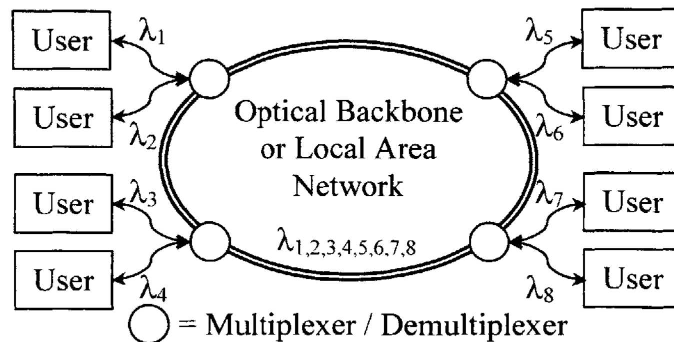

Figure 1.1: An implementation of WDM

However, WDM systems that exist today have high initial cost due to the high price and difficulty in fabricating the discrete optical components that make up the physical network. The heart of WDM is in the optical filter called a multiplexor, which adds and drops bands of wavelengths (more commonly referred to as channels) from the fiber. The ability to create a multiplexor that is small, easy to manufacture, and cheap would have a big impact on the widespread use of optical networks.

1.2 Planar Fabrication

Fabrication using planar techniques that the semiconductor industry has been using for decades can achieve small, easy to manufacture, and cheap optical devices. Semiconductor processing facilities have consistently produced reliable transistors with feature sizes on the order of tens of nanometers that are fabricated in parallel on large semiconductor wafers, which drives down the price of each device.

Semiconductor planar fabrication relies on a process that is based on techniques used for thousands of years. It involves coating a substrate with a polymer that reacts when exposed to irradiation from photons or electrons or when exposed to some liquid or gas. A mask that can block the irradiation or external substances is used to expose a pattern onto the polymer. This process is known as lithography.

The polymer is then developed in a solution that either removes the areas that have been exposed if positive resist were used, or have not been exposed if negative resist were used. Any processing that follows is known as pattern transfer. Material can be deposited on top filling in the exposed areas. The polymer beneath is then "lifted off" by being dissolved away leaving only the mask pattern behind. Alternatively, the substrate exposed by the polymer can be etched away, leaving behind an embedded mask pattern. The polymer is then subsequently stripped away.

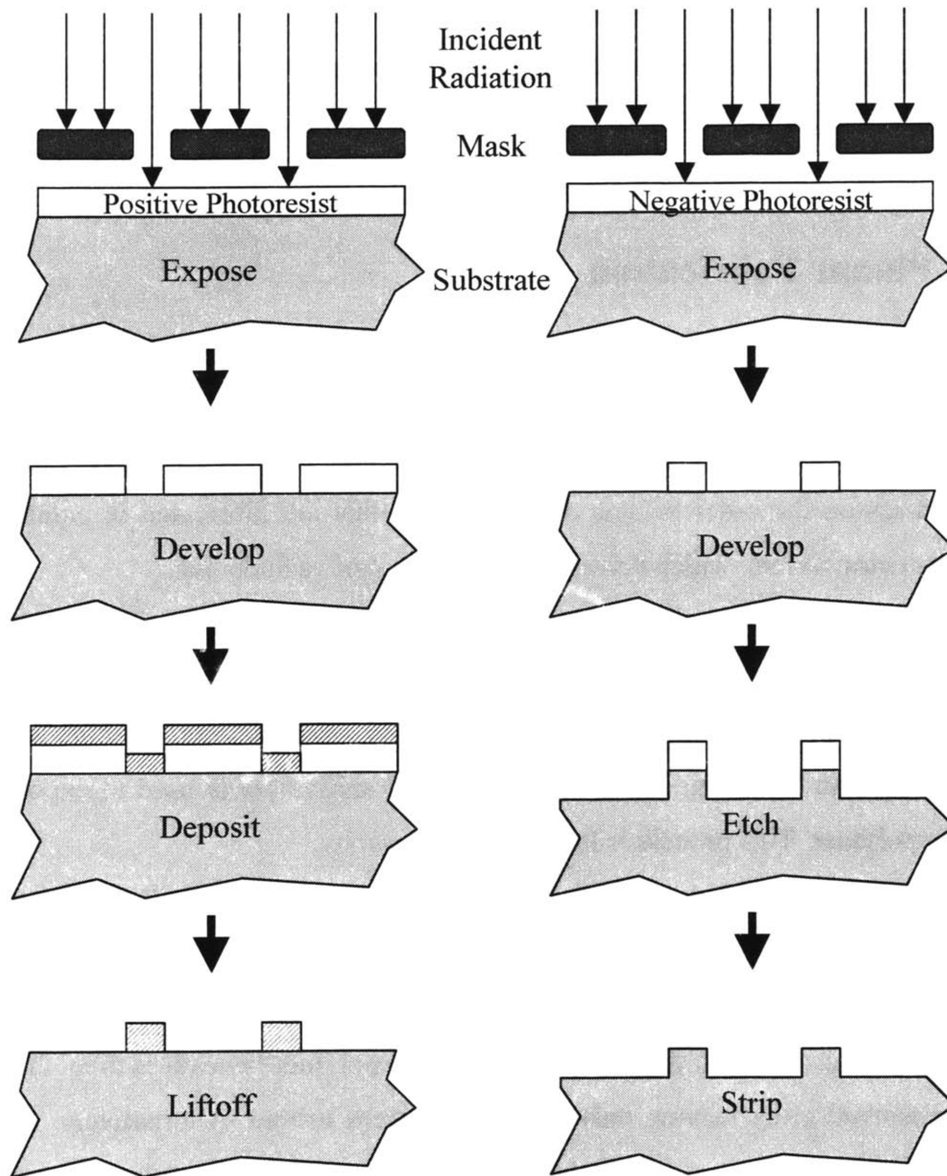

Figure 1.2: Planar Processing at a Glance

The most common planar optical filters consist of waveguides either in a ridge or channel structure. Material systems that have been used range from InP, GaAs, to Si. However, ultimately, these optical filters need to interface with existing optical networks via circular silica based optical fiber. Because of the shape of the optical fiber, the shape and size of the planar waveguide must be taken into consideration to maximize the power coupling into the planar waveguide. The reason for choosing to fabricate channel waveguides is that the shape closely matches that of optical fiber. The refractive index of the core and cladding should also closely match that of optical fiber for the same reason.

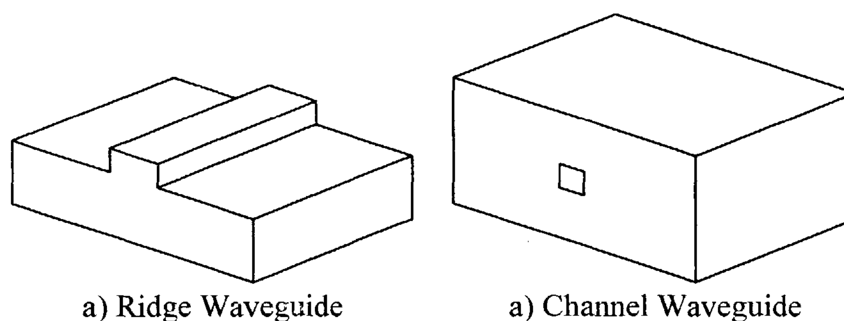

a) Ridge Waveguide a) Channel Waveguide

Figure 1.3: Ridge and Channel Waveguides

1.3 Bragg Gratings

Bragg gratings refer to an optical device that contains a periodic index modulation or structural corrugation that reflects light in a narrow band of wavelengths [3]. The longer the grating is, the stronger the reflection. The period and index contrast of the grating determine the wavelengths that are reflected. Such a property makes Bragg gratings ideal for use in WDM systems for selecting and picking off specific channels from a fiber. Since gratings can be realized by etching into a core of a planar waveguide using reactive ion etching (RIE), planar fabrication techniques can be used.

Bragg gratings are rapidly finding their place in discrete optical devices. They can be found in fiber Bragg gratings in which the index contrast of the fiber is induced by UV exposure of a standing wave. Fiber Bragg gratings perform the function of an add/drop channel filter, but the drawback is in the long lengths needed to achieve low transmission of the dropped channel. This is due to the low index contrast of the fiber. Having the

flexibility of selecting the refractive index using silicon oxynitride, we can fabricate Bragg gratings with shorter lengths.

Chapter 2

Process Overview

2.1 Add/Drop Channel Filter

The add/drop channel filter being fabricated is considered to be an integrated optical device, meaning that it is composed of discrete components tied together on one platform. The two main components are the coupler and the Bragg grating. Figure 2.1 provides a top down view of what the device looks like.

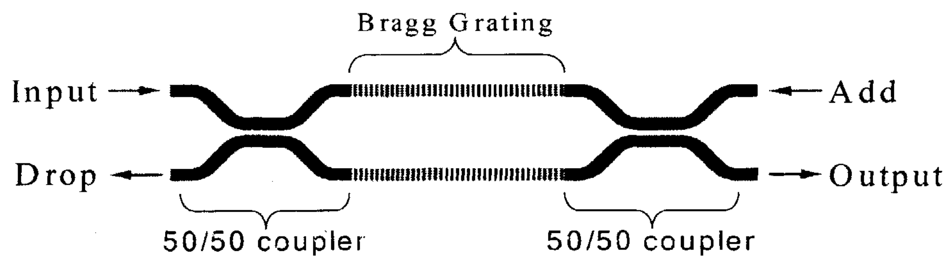

Figure 2.1: Add/Drop Channel Filter

The coupler acts as a device to transfer power from one waveguide to another. Depending on the distance the two waveguides and how long the coupling length is, a percentage of power will be transferred effectively splitting the signal [3]. In this case, the coupler is designed to split the input power by 50%. The Bragg grating reflects a band of wavelengths in the reverse direction on both arms back into the coupler. The coupler then completes the power transfer leaving 100% of the signal in the other waveguide, directing the reflected wavelengths to the drop port.

The remaining wavelengths will continue to travel through the Bragg grating into the second coupler, completing the power transfer, leaving the output port. Since this device is symmetric, you can replace the wavelengths that were dropped out through the add port which would get reflected into the output port.

There are several issues regarding each of the components and various designs to compensate for them. For instance, if the couplers were to remain what is shown in

Figure 2.1, they would only provide 50% power transfer for a given wavelength. Wavelength insensitive couplers have been designed in previous work done in NSL [4].

2.2 Process Flow

Figure 2.3 depicts an overview of the process flow to fabricate planar Bragg grating based optical filters. The process flow is explained in greater detail in Chapter 3.

This process flow will be explained in greater detail in Chapter 3.

2.3 Dual Layer Hard-mask

One of the major triumphs of the process flow is in the dual layer hard-mask approach to creating these optical devices. It was developed within NanoStructures Laboratory to solve the problem of creating gratings on top of relatively tall waveguide structures. The obvious approach to patterning gratings on top of a waveguide is to first create the waveguide, spin photoresist on top, and then expose a grating pattern.

Spinning photoresist on top forms an uneven layer that will expose at different rates when patterning the grating yielding varying duty cycles. Also, gratings are now present everywhere, not just on top of the core. Removing the extraneous gratings requires another alignment and exposure step.

The alternative is to utilize the dual layer hard-mask process. By patterning two hard-masks, the grating mask first and the waveguide mask on top, the planar surfaces used to expose the patterns are taken advantage of [5]. As an added bonus, this process provides self alignment to the grating pattern, allowing only the top of the core to have gratings.

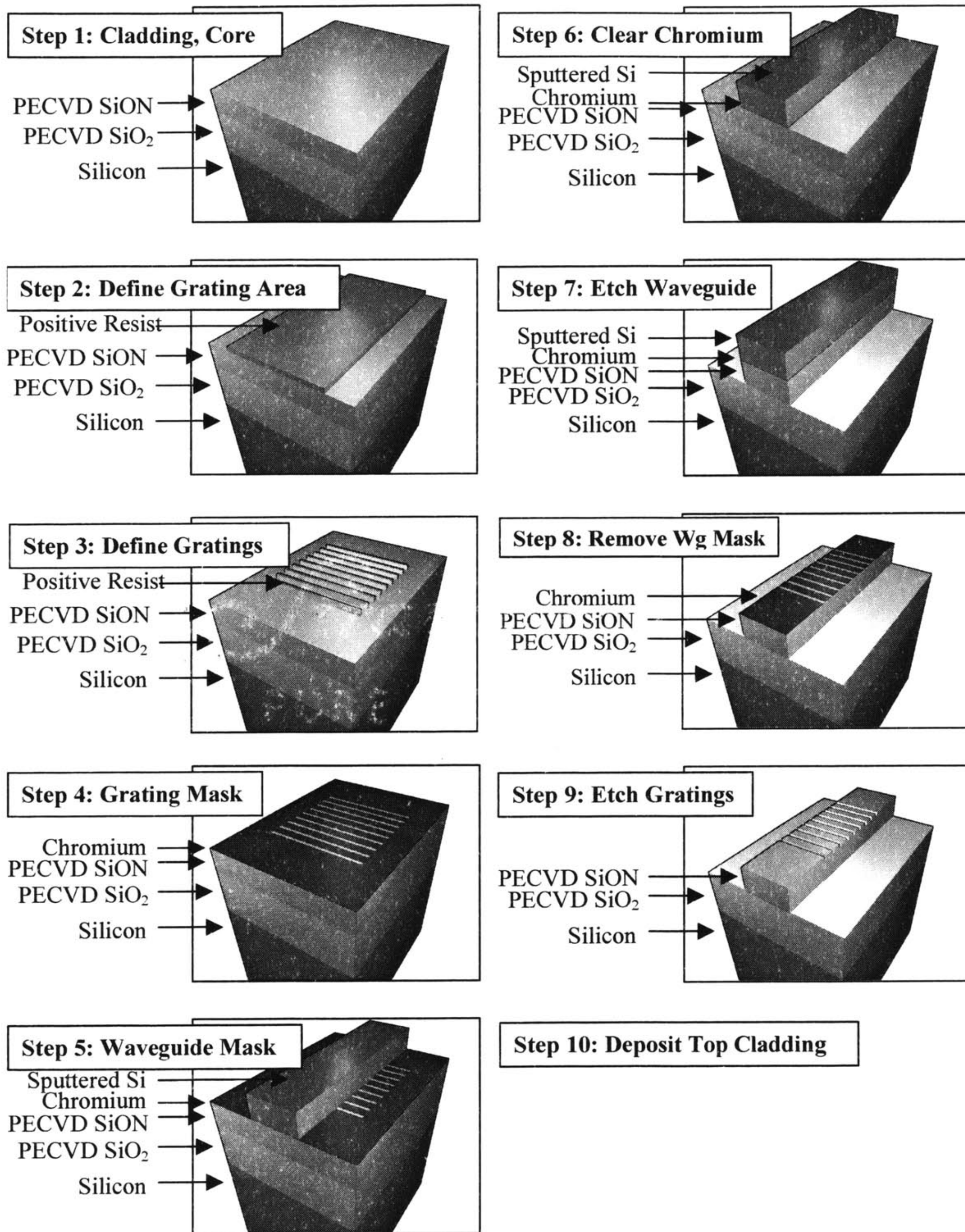

Figure 2.2: Process Flow

Chapter 3

Design and Fabrication

The goal of this chapter is to provide all the necessary information to design and fabricate glass channel Bragg grating based optical devices in silicon oxynitride. Theory as well as fabrication issues will be discussed hand-in-hand in a step-by-step process.

Many references exist that describe completely the phenomenon of electromagnetics and its mathematical representation in Maxwell's equations [6,7]. By briefly describing the fundamentals, we hope to give the reader some feeling as to why parameters were chosen in the final design of the device. We encourage the reader to refer to previous work and references for more in-depth discussions on electromagnetic theory and coupling theory.

Section 3.1 will describe the basic theory of waveguides necessary for choosing the lower cladding and core. Discussions in plasma enhanced chemical vapor depositions, subsequent annealing, chemical mechanical polishing, and measurement of these films will follow

Section 3.2 will describe the basic concepts of Bragg gratings needed to define the grating period. Discussions on the use of interference lithography and the Lloyd's mirror setup and measurement of the gratings will be presented.

Section 3.3 will go into basic coupling theory and bending loss necessary for the generation of the waveguide structures defining the couplers, grating region, and input/output ports of the devices.

Section 3.4 will talk about the series of reactive ion etching steps needed for etching the hard-mask layers, deep etch of the waveguides, and finally, the grating regions.

Section 3.5 will then talk about the theory of resputtering and its benefits in filling in the voids in high aspect ratio gratings and waveguide structures using ECR plasma enhanced chemical vapor deposition.

3.1 Lower Cladding and Core Deposition

3.1.1 Dielectric Waveguides

Dielectric waveguides are non-conductive optical conduits that can guide light to a destination. The condition for guidance resides in the refractive index of the materials the waveguide is composed of. For example, an optical fiber is composed of a glass core with a refractive index higher than the refractive index of the cladding surrounding it. Total internal reflection guarantees that the light will be confined within the waveguide provided that the light bounces off the core/cladding boundary at an angle greater than the critical angle derived from Snell's Law. A geometric optical model can be seen in Figure 3.1.1.

$$\text{Critical Angle } \vartheta_c = \sin^{-1}\frac{n_{clad}}{n_{core}} \qquad (3.1)$$

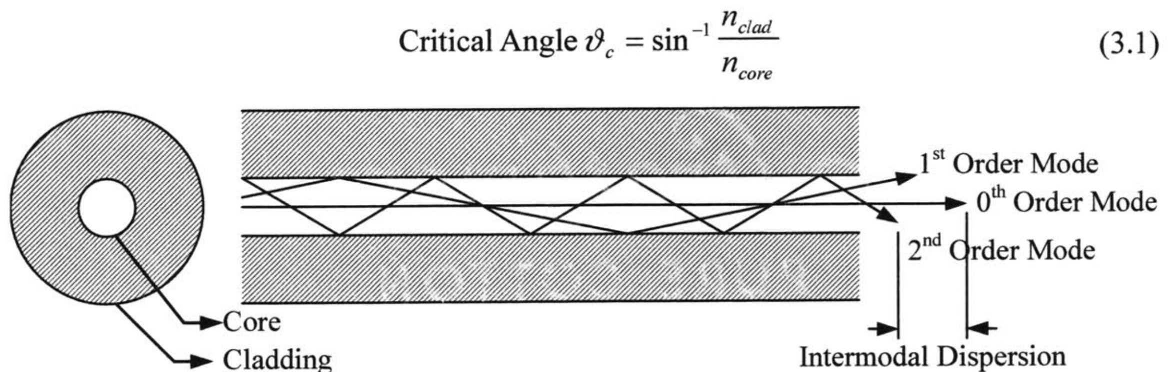

Figure 3.1.1: Geometric optical fiber model

Several modes may propagate through a fiber for a given wavelength, each with a different projection of the k vector onto the core axis. If we send an input signal using one mode at a particular wavelength, it may excite the other modes, with each mode appearing at the destination at different times due to the varying propagation velocities. The received signal would then become smeared in time resulting in an upper limit to how fast data can be transmitted [20]. An example of intermodal dispersion is shown in Figure 3.1.2.

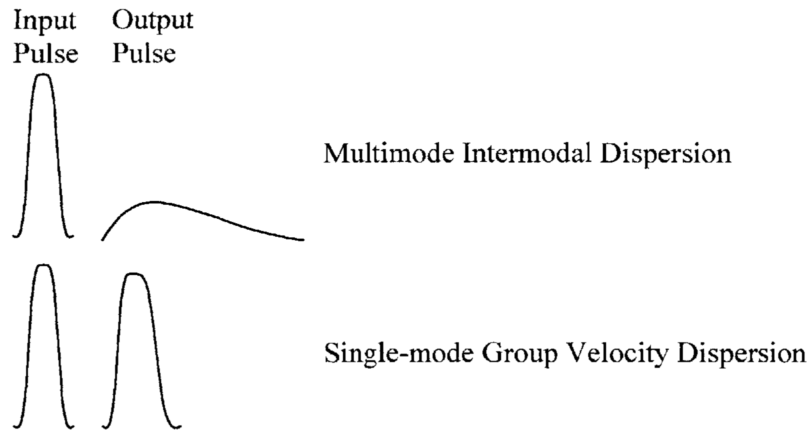

Figure 3.1.2: Pulse Dispersion

One way of solving the problem of intermodal dispersion is to limit the number of modes that can propagate through the fiber. We can do this by shrinking the diameter of the core. By decreasing the number of allowable propagating modes to just the lowest order mode, we get a single-mode waveguide. There are other forms of dispersion that can affect single-mode pulses, but their effects are mostly due to the material being used and the laser producing the pulse.

The first thing in the design criteria for the material of the core and cladding of the waveguides of an optical device is to consider the size of the core to guarantee a single-mode waveguide. However, because we are working with rectangular waveguides, no simple closed form solutions to Maxwell's equations exist. This fact preempts the use of analytical software in order to solve for the propagating modes and their propagating constants to determine what the size of the core should be.

However, there is a tradeoff to how small the core can be. These devices will eventually have to be attached to a single-mode optical fiber whose core diameter could range from 8-10um. Making the core too small would transmit less light into the device. The rest of the light would radiate away into the cladding. Thus, the challenge is to calculate the largest size core while still being single-moded.

We used MATLAB code that utilized a finite difference method approach to determining the mode profiles of all the allowable propagating modes as well as the effective refractive index for each mode [4,8,9]. After calculating for the propagation

constants for the mode, we can determine the effective refractive index of the waveguide through this simple equation.

$$n_{eff} = \frac{\beta\lambda}{2\pi} \tag{3.2}$$

β is the propagation constant of the waveguide, λ is the wavelength of the light traveling through the waveguide, and n_{eff} is the effective index of refraction. If the propagation constant were referring to a slab waveguide (an infinite planar core sandwiched between two cladding layers), the effective index of refraction would be the slab core's refractive index. The index profile is translated to a slab waveguide for the purposes of calculation simplicity.

3.1.2 Plasma Enhanced Chemical Vapor Deposition

In previous work, the cladding and core were acquired from outside sources. Lower cladding layers were either formed by flame hydrolysis or high-pressure steam oxidation (HiPOX). The core was formed using chemical vapor deposition (CVD) techniques with phosphorous doping to obtain the desired index contrast [4]. However, suppliers of thick oxides on silicon substrates were no longer available due to business restructuring and conflict of interest. The ability to deposit our own cladding and core became a necessity. As will be discussed in Section 3.5, a material change was also required to solve the difficulties in depositing the top cladding.

The search for a new material for a glass channel device generated the following criteria.

- Ability to change the refractive index
- Reasonable rates of deposition
- Ability to resist melting and diffusion during top cladding deposition
- Low loss for the 1550nm infrared wavelength window
- Easily obtainable on campus

Several material systems were contemplated. Thermal growth of oxides takes too long to grow silicon dioxide, flame hydrolysis tools were unavailable, and phosphorus doped cores has low melting temperatures. The material that was settled upon is silicon oxynitride.

Silicon oxynitride (SiO_xN_y or SiON), a blend of silicon dioxide and silicon nitride, can be deposited using sputtering deposition or plasma enhanced chemical vapor deposition (PECVD). This material was chosen for the following reasons.

- Refractive index can be changed from that of oxide to that of nitride (1.46-2.00)
- The Novellus Concept-One, a PECVD tool, can deposit 10um of oxide in 20 min
- The melting temperature of SiON is higher than the deposition temperature
- Low loss for the 1550nm wavelength is attainable after annealing [12]
- PECVD tools exist on campus and are easily accessible

PECVD silicon oxynitride films combine some of the best properties of plasma silicon nitride and oxide films. The presence of oxygen lowers the stress, dielectric constant, and refractive index, while the presence of nitrogen increases the resistance to the diffusion of sodium ions, moisture, and other contaminants into the SiO_2 network [16].

The major advantage that PECVD has over thermally driven CVD is the lower operating temperature of deposition with high growth rates while still maintaining high quality films. For example, thermal CVD operates at 700 to 900°C, whereas only 250 to 350°C is sufficient for PECVD. The lower temperature is made possible by the substitution of the electrical energy provided by the plasma for the thermal energy.

Deposition of the lower cladding and core were done using the Novellus Concept-One. This tool normally deposits oxides and oxynitrides at 400°C through five separate deposition stations, producing an averaging effect that decreases formation of pinholes, provides better uniformity, and gives higher throughput. The tool also allows separate manipulation of the high frequency plasma excitation RF (used for controlling the amount of reactive species in the atmosphere) and the low frequency RF (used for conformity and stress control of the film) [17].

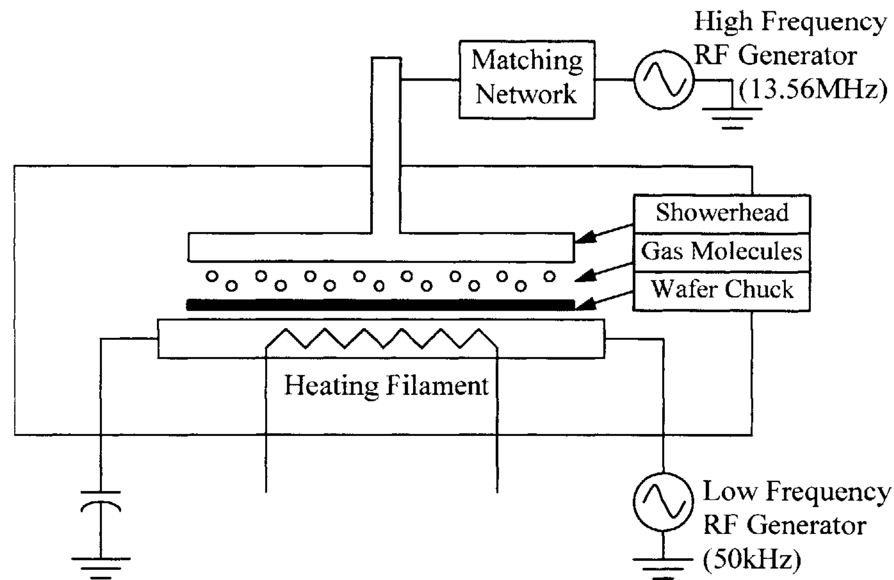

Figure 3.1.3: Single Novellus Concept-One Deposition Station

To deposit oxide, a gas mixture of SiH_4 (silane), N_2O (nitrous oxide), and N_2 were used. Nitrogen-diluted silane serves as the silicon source, while nitrous oxide provides the oxygen. Nitrous oxide is most commonly used in PECVD as an oxidizer because of the relatively low (1.7eV) bond dissociative energy of N—O in this molecule. As will be discussed in Section 3.5, a gas mixture of SiH_4, and O_2 can be used, but the gas mixture is considerably more reactive yielding worse uniformity and more particle contamination than SiH_4-N_2O films [16]. In essence, $SiH_4+N_2O = SiO_2 + H_2O + 2N_2$. Actual molecule formations will be discussed further in the next section.

To deposit oxynitride, NH_3 is injected into the chamber. Changing the ratio of N_2O to NH_3 will affect the concentrations of oxygen and nitrogen in the deposited film. To obtain low index contrasts to PECVD oxide, a high ratio is needed.

As can be imagined, many parameters can be tweaked in a PECVD system. Figure 3.1.4 shows what effects modifying certain parameters has on the deposited film. Removal of the low frequency RF allows for increased rate of deposition, better wafer thickness uniformity, as well as less tensile stress. Reasons for this has to do with the phenomenon of resputtering that will be discussed in further detail in Section 3.5.

Run Conditions		Uniformity	Deposition Rate	Refractive Index	Film Stress
Effect of increasing	RF Power	↓	=	↓	↓
	Pressure	↑/↓	↑/↓	↓	↓
	N_20/SiH_4	=	↑	↓	↓
	N_2	↑	↑	↑	↑
	SiH_4	↑	↑	↑	↑
	NH_3/SiH_4	↓	↑	↑	=

↑ Value increases; uniformity worsens; film becomes more tensile
↓ Value decreases; uniformity improves; film becomes more compressive
↑/↓ Value increases (uniformity improves), passes through optimum, then decreases (worsens).
= Value remains the same, or the change is negligible (<10%)

Figure 3.1.4: Effects of changing PECVD parameters [17]

3.1.3 Annealing

A drawback to PECVD films is that they are composed of an amorphous mixture of molecules. Because of the use of SiH_4, PECVD oxides also contain Si—H, Si—O—H, and H—O—H bonds along with the expected SiO_2 bonds. For PECVD oxynitrides, there is the additional presence of N—H bonds [10]. Unfortunately, the vibrational overtones of Si—H and N—H bonds cause optical loss at about 1.8dB/cm at 1500nm and 0.4dB/cm at 632.8nm wavelengths [12]. Increasing the presence of N_2O can reduce the presence of Si—H. However, high temperature annealing is required to drive out the hydrogen content. Doing so can reduce the optical loss of low-index PECVD SiON to less than 0.2 dB/cm at the 1550nm wavelength [11].

FTIRAS (Fourier Transform Infrared Absorption Spectroscopy) measurements have been made on PECVD SiON films and it has been shown that annealing at high temperatures lowers overall hydrogen content. Films annealed from 850-1000°C have their N—H bond concentrations decrease considerably faster than Si—H bonds. During the high temperature annealing, the reaction Si—H + N—H → Si—N + H_2 can occur as well as the formation of Si—Si bonds which can yield silicon rich oxides [15].

During annealing, the permeability of oxide readily allows the outdiffusion of hydroge. It should be noted that nitride films are considerably less permeable than oxides.

High temperature annealing of PECVD nitrides may destroy the film resulting in blistering of the film [16]. Thus, PECVD oxynitride films with high nitride content will output wafers that will appear shattered after annealing. Figure 3.1.5 is an example of this. Shattering is not a concern for these devices since we are only interested in refractive indices closer to oxides.

Another drawback to PECVD films is the stress formed during deposition. Nitrides and high refractive-index oxynitrides crack under excessively high compressive stress and can easily crack under tensile stress. However, the use of dual RF frequency deposition techniques, which the Concept-One employs, can be used to control film stress at the cost of worsened uniformity. Low excitation frequencies (such as 50kHz) tend to yield films with compressive stress while the use of high excitation frequencies (13.56 MHz) may yield films with tensile stress. However, oxides and low refractive index oxides can be deposited with just the use of high excitation frequencies while maintaining low compressive stress and retaining good wafer uniformity.

PECVD films can also be etched faster than thermal CVD films in wet etch as well as dry etch chemistries. That is why annealing is commonly done to densify PECVD films. The process of driving out the hydrogen bonds decreases the thickness of the films and increases the refractive index as a result.

Figure 3.1.5: Stress of high refractive index silicon oxynitride after annealing

3.1.4 Chemical Mechanical Polishing

After depositing oxide and oxynitride films on a silicon wafer using PECVD, the surface of the films have noticeably rough surfaces easily detectable when viewed with a scanning electron microscope (SEM). Surface roughness has been measured to have a 35nm mean, with 50nm from peak to peak for a 10um PECVD oxide deposition without annealing. Figure 3.1.6 shows an atomic force microscope (AFM) scan of a 4um square area.

Subsequent annealing only removes sharp points that may have formed. But the majority of the surface roughness still remains. Even though a 50nm peak may not introduce much loss, it still is a contributor. Roughness can be easily removed with the use of chemical mechanical polishing (CMP).

CMP is mostly used to planarize structures that have been filled in with a sacrificial material. It can also be used to planarize thin films such as oxides, nitrides, and polysilicon. It involves taking the wafer and applying force onto a pad with slurry that polishes the surface with minute colloidal silica suspended in a liquid. The result is a surface that has sub-nanometer roughness that only the AFM can detect. The drawback is that if the slurry is not washed off the wafer, it will dry and stick like cement. Subsequent cleaning is a feat in itself with much literature devoted to the analysis of the pH of the slurry and solutions to wash the slurry off. A routine piranha clean is done to ensure removal of the slurry off the surface of the film. Figure 3.1.7 shows SEM images before and after CMP of an SiON deposited film.

3.1.5 Measurement of Thin Films

Two properties of the PECVD films are crucial in the design of the devices: the refractive index at 1550nm and the thickness. There are many tools that can measure these parameters, but only two are capable of measuring both at the same time.

- Ellipsometer with a fixed 1550nm wavelength laser
- Metricon with a fixed 1554nm wavelength laser

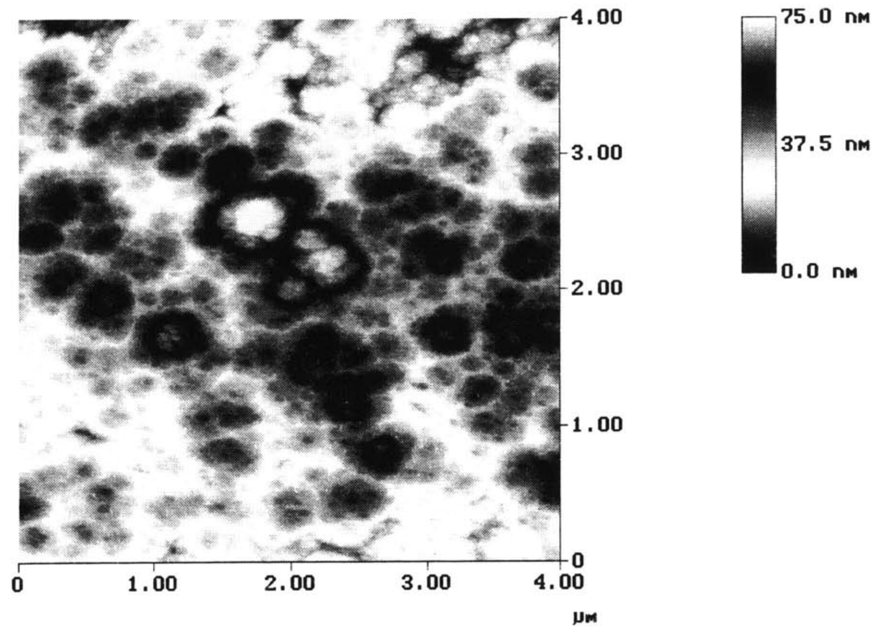

Figure 3.1.6: AFM scan of 10um PECVD oxide unannealed

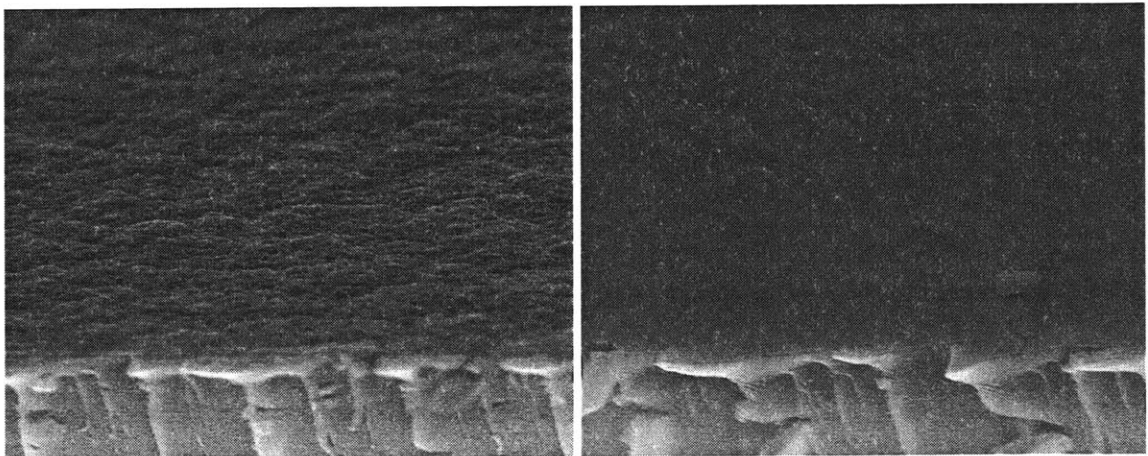

Figure 3.1.7: SEM image of a PECVD SiON film before (left) and after (right) CMP

Ellipsometers are excellent metrology tools for measuring refractive indices and thicknesses at the same time. However, due to the oscillatory nature of the measured parameters, the thickness measurement is generalized and multiple thicknesses will be given. Measuring the thin film at multiple angles can narrow the result to one thickness, but the measurement can be deceiving or may give no answer if the film is highly birefringent or highly absorbent. Another type of ellipsometer is known as a spectroscopic ellipsometer. It is capable of sweeping across multiple wavelengths giving deep insight into the properties of the film being measured. But the main reason for not using an ellipsometer was that no ellipsometer equipped with a 1550nm laser was available.

A Metricon tool was available on campus and provided a means for simultaneously measuring the refractive index and thickness of a film. Figure 3.1.8 shows an overhead view of the Metricon. Operation requires the film to come into contact with a prism of higher refractive index. The prism and film is rotated as a fixed laser is shone on the prism. Due to total internal reflection, all the incident radiation should be reflected into the photo detector.

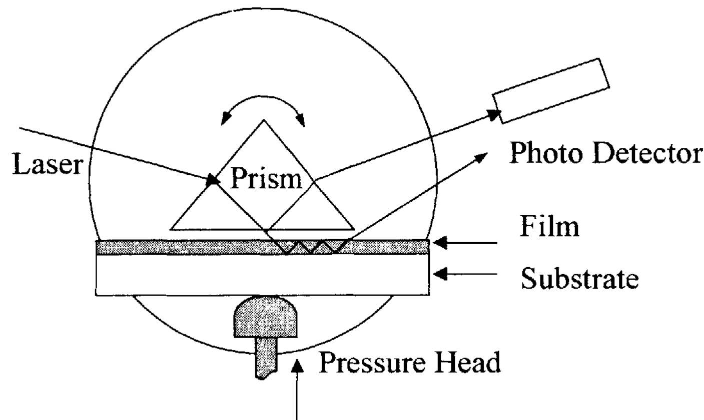

Figure 3.1.8: Metricon Overhead Diagram

However, there are certain angles of incidence where the laser will couple into the film and propagate within the film. The exponentially decaying radiation that usually travels on the boundary of the prism and film is transmitted via coupling into the film, and after some distance of reflection between the substrate and film, is coupled back into

the prism. When this occurs, the photo detector will reveal less reflected radiation than it normally does. The refractive index and thickness can be calculated from the angle at which this at which these dips occur, provided that at least two modes are present. More than two modes provide a means for verification of the measurements.

However, if the air gap between the film and prism becomes too small, a overcoupling occurs. For single films on high index substrates such as silicon, overcoupling can degrade measurement accuracy (especially thickness accuracy) by causing a slight shift of the mode angle positions. The shift in mode positions can result in a calculated film thickness that is as much as 5-7% less than the true film thickness. Overcoupling effects on film index are generally slight (less than .002 even in severe cases) for single films. By lowering the pressure between the film and the prism, overcoupling can be overcome [18].

Being the only tool within easy access for measuring the PECVD oxide and oxynitride films, the only means for verification of the validity of its measurements were in the Metricon's capability to measure refractive indices at the 632.8nm and 1307nm wavelengths. Comparisons between the Metricon and ellipsometers at the 632.8nm wavelength yielded similar results. Thicknesses were doubly verified from cross sections in an SEM.

Figures 3.1.9-3.1.11 lists the major results of the measurements done by the Metricon for the Concept-One PECVD films used for fabricating the optical devices.

	Before Anneal		After Anneal	
	Thickness	Refractive index at 1554nm	Thickness	Refractive index at 1554nm
PECVD SiO2	10.11um	1.4518	9.61um	1.4525
PECVD SiON	3.54um	1.4589	3.44um	1.4793

Figure 3.1.9: Measurements of PECVD films before and after annealing

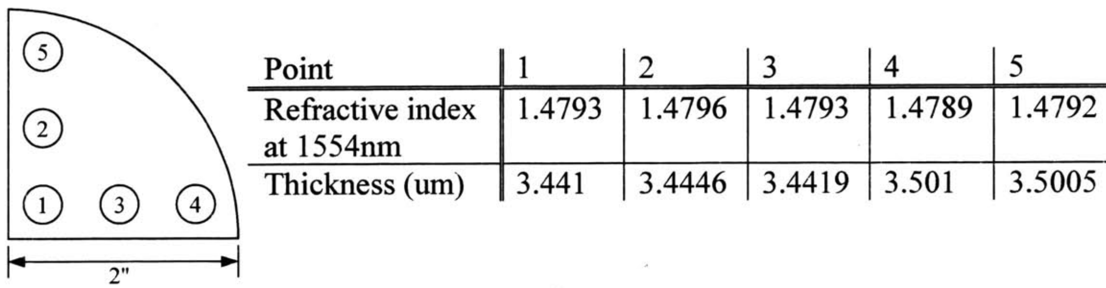

Point	1	2	3	4	5
Refractive index at 1554nm	1.4793	1.4796	1.4793	1.4789	1.4792
Thickness (um)	3.441	3.4446	3.4419	3.501	3.5005

Figure 3.1.10: Uniformity Measurements of PECVD SiON film after annealing

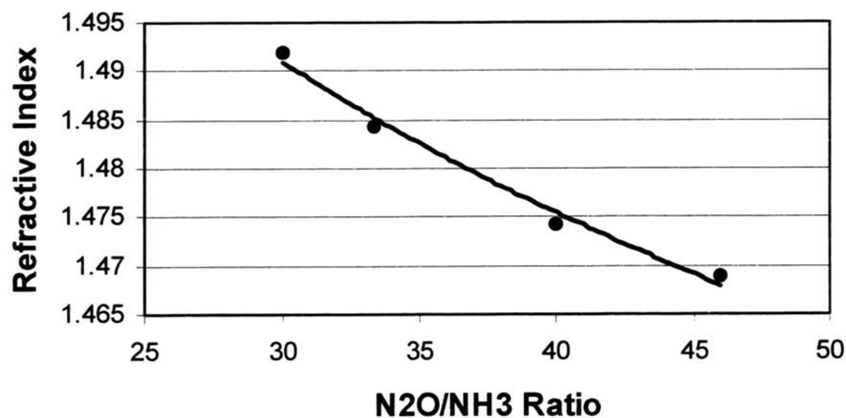

Figure 3.1.11: Refractive Index with 0.3sccm SiH_4, 1.6sccm N_2, 1.1kW HF, 0kW LF

3.1.6 Processing

The following is a step by step process of what was done for fabrication.

1. Piranha Clean Silicon wafer

   Since the Novellus Concept-One requires strict rules for what can enter the chamber, all wafers that came from outside the fab must be cleaned by a two step piranha clean.

   A. Dip wafer in 1:3 H_2O_2:H_2SO_4 for 10 minutes

   B. Dip wafer in a new solution of 1:3 H_2O_2:H_2SO_4 for 10 minutes

   C. Dip wafer in 50:1 HF for 15 seconds

2. Deposit 10um of SiO_2 using Novellus Concept-One. The recipe used is as follows.

1.5 sccm	N_2
0.3 sccm	SiH_4
9.5 sccm	N_2O

1.1 kW	High Frequency Power
0 kW	Low Frequency Power
2 T	Pressure
400 C	Temperature
240 s	Time per station
2400 A/m	Deposition Rate
5540 A/m	Etch Rate
120 s	Precoat
0.5 s	PreA Delay
0.5 s	PostA Delay
0 s	TEOSRF Delay
10 s	Temp Soak
0	X Value
300	Y Value

Figure 3.1.12: Concept-One Recipe for 10um of n=1.4525 SiO_2

Note: The Deposition Rate and Etch Rate values are only used for the purpose of the clean step that is always run after all the wafers have been deposited. It determines how long the clean step should be run for. An endpoint detection system would nullify the necessity for specifying these values.

3. Densify in annealing tube at 1100°C for 3 hours (30 minute ramp up, 90 minute bake, 1 hour cool down)

4. Polish wafer with the Strasbaugh CMP using the following settings.

30 sec	Time
25 RPM	Table speed
25 RPM	Quill speed
3.5 psi	Down Force
100 mL/min	Slurry Output
1.0 psi	Back Pressure

Figure 3.1.13: CMP Recipe for Planarization

5. Piranha clean wafer without HF dip

   Since we want to preserve our PECVD film as much as possible, no HF dip is permissible.

   A. Dip wafer in 3:1 H_2O_2:H_2SO_4 for 10 minutes

   B. Dip wafer in a new solution of 3:1 H_2O_2:H_2SO_4 for 10 minutes

6. Deposit 3.36um of SiON using Novellus Concept-One. The recipe used is as follows.

1.6 sccm	N_2
0.3 sccm	SiH_4
12 sccm	N_2O
0.3 sccm	NH_3

1.1 kW	High Frequency Power
0 kW	Low Frequency Power
2 T	Pressure
400 C	Temperature
240 s	Time per station
2400 A/m	Deposition Rate
5540 A/m	Etch Rate
120 s	Precoat
0.5 s	PreA Delay
0.5 s	PostA Delay
0 s	TEOSRF Delay
10 s	Temp Soak
0	X Value
300	Y Value

Figure 3.1.14: Concept-One Recipe for 3.44um of n=1.4793 SiON

7. Repeat Step 3: Densify in Annealing Tube
8. Repeat Step 4: CMP SiON thin film
9. Repeat Step 5: Piranha Clean without HF dip

3.1.7 Summary

Silicon oxynitride films were chosen to be the core material because of the availability of PECVD tools, the literature available, and the optical devices that have previously been fabricated using it. Characterization of PECVD films were done to deposit oxide and oxynitride films that have the good thickness and refractive index uniformity as well as low index contrast. The Novellus Concept-One PECVD system had high repeatability and was capable of depositing 10um of oxide in 20 minutes.

Subsequent annealing was required to drive out hydrogen content from the film that is inherent from PECVD processing. Annealing at 1100°C was performed to reduce the optical loss caused by the hydrogen bonds with oxygen and silicon. Stress of the films were not a concern since cracking of the oxynitride films only occur indices of refraction approaching that of nitride. CMP was also employed to smooth the surfaces of the films to minimize on loss.

Measurements of these films were made using the Metricon that was the only tool that was accessible to measure films at the 1554nm wavelength. After understanding and mastering the flaws that the Metricon has in overcoupling, an oxynitride based material system was established for the fabrication of optical devices without the need for outsourcing material.

3.2 Bragg Grating Hard-mask Definition

3.2.1 Grating Strength

The mechanism that performs the add/drop function of this device is known as a Bragg grating. A Bragg grating is a periodic structure that scatters radiation generating constructive interference [19]. In the case of this device, the grating is placed on top of the core, reflecting a portion of the incoming radiation over a long distance. The wavelength that gets reflected is determined by the period of the grating. The reflected radiation constructively interferes only for a particular band of wavelengths. The remaining radiation is transmitted on the other side of the grating region.

In order for constructive interference to take place, the path difference between reflected light paths must be an integral number of wavelengths. Strongest reflection occurs at wavelength λ_0 when the grating period is half of λ_0/n_{eff}.

$$\Lambda = \frac{\lambda_0}{2n_{eff}} \tag{3.2}$$

n_{eff} is the effective index that the incoming radiation sees. Since the refractive index profile is composed of a rectangular core surrounded by a cladding, the effective index will reside somewhere in between the two contrasting indices. This value was calculated when we were determining the thickness of the core to guarantee single mode operation.

Figure 3.2.1 shows a simplified picture of how the reflections take place. Internal reflections between grating teeth have been ignored, but it turns out that a large percentage of the radiation is reflected back out of the grating region.

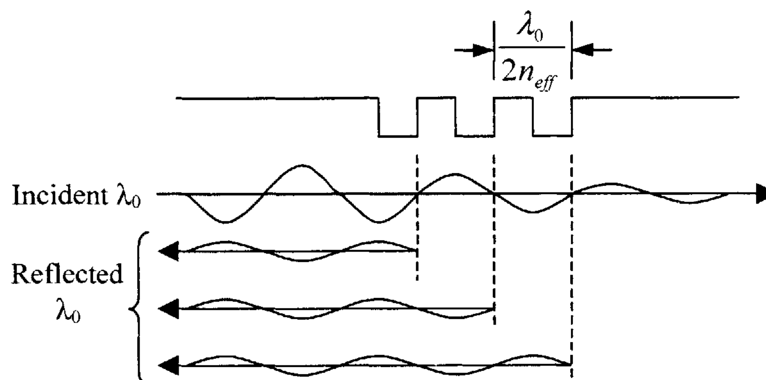

Figure 3.2.1: Reflection and Transmission of Bragg Grating

There are some issues with using Bragg gratings that should be addressed.

- The reflected pulse is convolved in time (a convolution with a square wave which represents the grating region). This limits the maximum bitrate that can be transmitted because the convolution extends the width of the signal. Intersymbol interference will occur if adjacent pulses intersect. However, the reflected pulse can still be easily recognized using matched filters [19].
- Since the gratings only overlap a portion of the incoming radiation, the grating region must be long to ensure transmission power suppression greater than 25dB, a typical requirement for channel dropping filters. Having long gratings also makes demands for chirp-free gratings. Gratings with chirp would have phase shifts or a gradual period change across the grating that would affect the spectral response of the optical device.
- The depth of the grating teeth plays a role by affecting the area the incoming radiation overlaps. Not only will increase depth provide stronger reflections, it will also reflect a wider band of wavelengths centered at the same wavelength as before.

The grating strength must be large enough to provide isolation between channels of transmitted data greater than 25dB suppression and a passband region to have less than 1dB of loss. Balancing the grating depth and length parameters provides design freedom in selecting a spectral response for a Bragg-grating-based optical filter.

The grating strength is quantified in a coupling constant κ, which has units of inverse length. It is referred to as a coupling constant since the incoming electromagnetic modes are actually coupling and exciting modes in the reverse direction [3]. Much thought has been put into the calculation of the grating strength and its effects on the reflection spectrum of the Bragg gratings. References are provided [3,4,21]. The following are the equations to calculate κ.

$$\kappa = \frac{k^2}{2\pi\beta}\left(n_{core}^2 - n_{clad}^2\right)\sin(\pi D)\Gamma \tag{3.3}$$

$$\text{where } \Gamma \equiv \frac{\iint\limits_{(grating)} |\phi(x,y)|^2 \, dxdy}{\iint |\phi(x,y)|^2 \, dxdy} \tag{3.4}$$

D is the duty cycle of the grating. $\phi(x,y)$ is the mode profile of the incoming radiation. Γ is the percentage of $\phi(x,y)$ that overlaps the grating region. β is the propagation constant for a given duty cycle and grating depth.

It must be noted that the refractive index profile changes as the grating depth changes. No longer does the grating region have the refractive index of the core. Perturbation theory can be used to approximate the grating region as an average of the core and cladding refractive indices weighted by the duty cycle [19,21]. Calculation for κ can be time consuming if one wants to generate plots for all different permutations of duty cycle and grating depths. Figure 3.2.2 portrays such a calculation for a 3.35um core.

Once κ is known for various grating depths, computation of the reflection spectrum from the Bragg gratings is done for various lengths of the device (L). κ and L are then chosen depending on the specifications of the filter being designed.

$$|r(\delta)| = \frac{\frac{\kappa}{\gamma}\tanh(\gamma L)}{1 - i\frac{\delta}{\gamma}\tanh(\gamma L)} \tag{3.5}$$

$$\text{where } \delta \equiv \beta - \frac{\pi}{\Lambda} \text{ and } \gamma \equiv \sqrt{|\kappa|^2 - \delta^2} \tag{3.6}$$

To determine the bandwidth that will be reflected, the following equation is used.

$$\Delta f = \frac{\kappa c}{\pi n_{eff}} \tag{3.7}$$

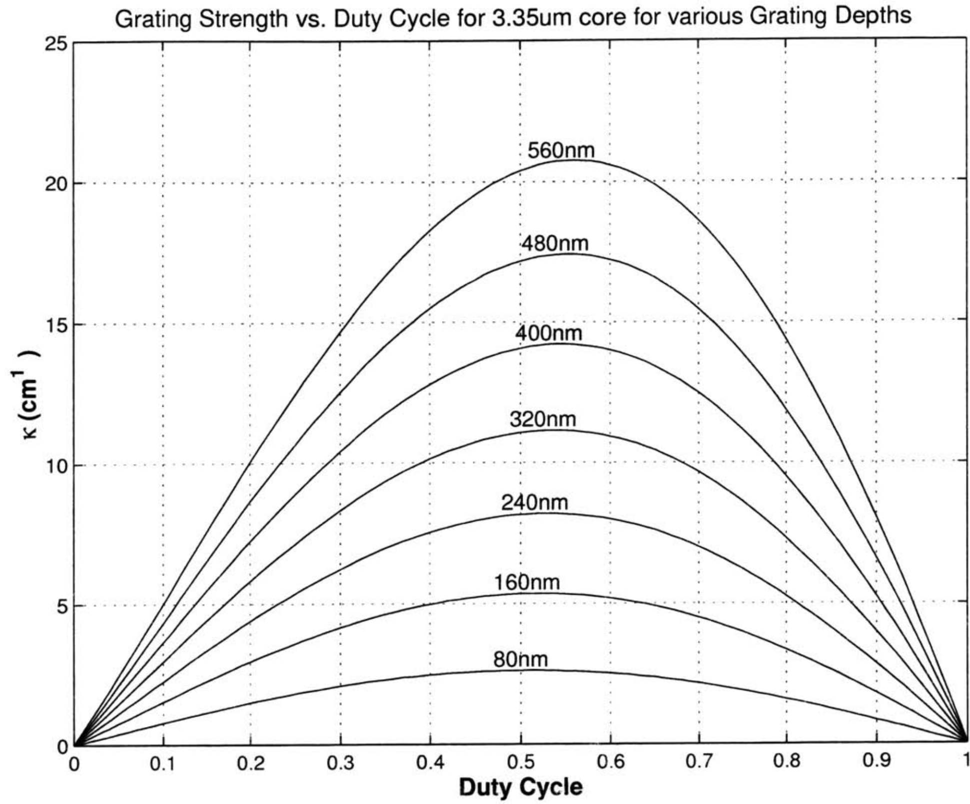

Figure 3.2.2: Example of a calculation for κ

For the device being fabricated in this thesis, Figure 3.2.3 shows a table of κ and the grating depth and the length of the grating required to obtain a κL = 6 for a 3.35um core.

Δf (GHz)	κ (cm^{-1})	Grating depth (nm)	L (mm)
50	7.67	222.1	7.824
60	9.20	261.9	6.520
70	10.74	301.6	5.589
80	12.27	341.3	4.890
90	13.80	381.1	4.347
100	15.34	420.8	3.912

Figure 3.2.3: κ, Grating Depth, and L Calculations for 3.35um core

3.2.2 Interference Lithography

There exists several ways to pattern the gratings needed. Electron beam lithography can direct write the grating in a raster-like fashion. However, the resulting grating would have intra-field distortion as well as stitching errors between fields [22]. SPLEBL, Spatial Phase Locked Electron Beam Lithography, is a method that can fix the errors that open-loop electron-beam lithography cannot resolve. However, electron beam lithography may be useful if a final mask was being written. For prototyping, a far more elegant solution exists to pattern long gratings four or more millimeters in length.

An alternative to direct writing is to use interference lithography (IL) in order to generate large areas of uniform gratings simultaneously. IL works by intersecting two light beams of the same wavelength. A standing wave results due to constructive and destructive interference. Changing the angle by which the beams overlap will form standing waves with different periods. Figure 3.2.4 depicts this scenario in a standard two beam setup where a wafer with photoresist is placed in the standing wave plane to absorb the intensity pattern.

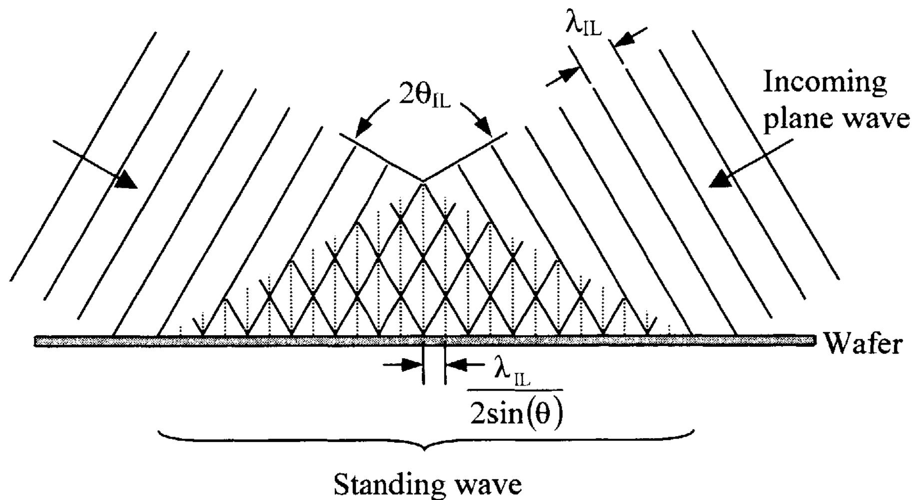

Figure 3.2.4: Interference Lithography

The following equation relates the angle θ with the desired period p, for the interference pattern.

$$p = \frac{\lambda_{IL}}{2\sin\theta} \tag{3.8}$$

There are some issues when using traditional two-beam IL that should be considered.

- In typical IL setups, the incoming wavefronts are usually spherical due to the use of spatial filters to create a large area of gratings at the same time. Spherical wavefronts introduce chirp into the interference pattern, with zero period shift at the center of the grating region and worsening as you move toward the edges.
- Lasers typically have beams with Gaussian intensity profiles. Depending on the photoresist used, the time required to expose the desired duty cycle would be shorter in the center of the interference region than near the edges. Expanding the beam to reduce the intensity difference just for a desired region would help, but at the expense of longer exposure times.
- Reflection off the wafer surface can create standing waves in the resist profile, which is undesirable for applications needing vertical sidewalls. The use of a tri-layer resist stack, composed of anti-reflection coating (ARC), and an SiO_2 interlayer between the ARC and resist, can reduce the reflection to nil. Calculation of the necessary thicknesses for the ARC and SiO_2 layers can be done using several methods, one of which applies transmission line theory to the dielectric stacks [23]. Figure 3.2.5 shows an SEM micrograph of a grating that was exposed on top of ARC and SiO_2.

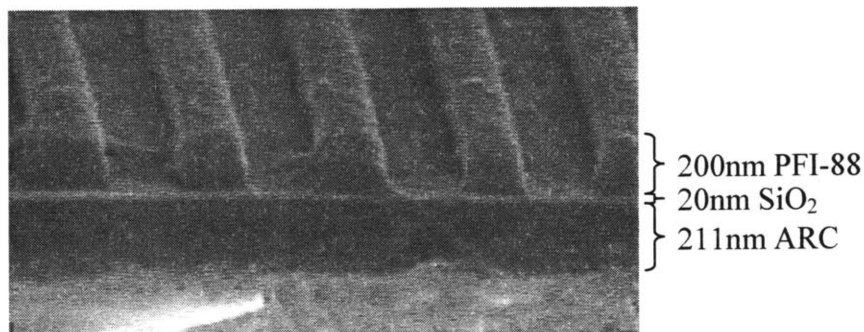

Figure 3.2.5: Grating developed in tri-layer resist

3.2.3 Lloyd's Mirror

There are many ways of implementing IL, three of which have been built at MIT: Achromatic Interference Lithography (AIL), a conventional Mach-Zehnder interference lithography, and a Lloyd's mirror [22]. The advantage of the Lloyd's mirror is in the quick setup time due to the simplicity of the design. The disadvantage is that on the wafer plane, the intensity of the beam reflected by the mirror is lower than the direct illumination. This creates exposures with varying duty cycles across the grating region. Figure 3.2.6 depicts this IL setup.

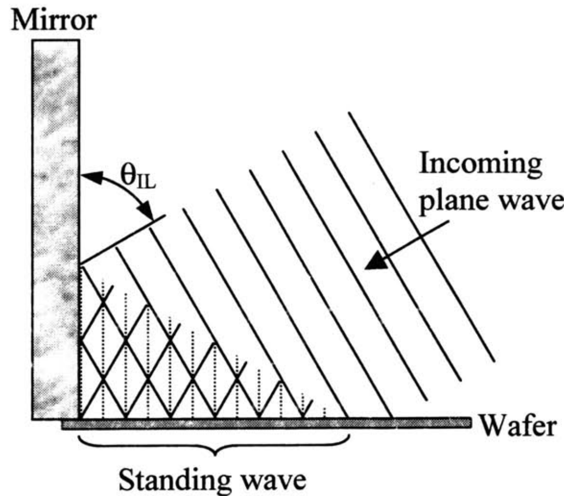

Figure 3.2.6: Lloyd's Mirror

The Lloyd's mirror is not meant to be used to produce precise gratings, but for quick samples with gratings. In the best interest of time to yield prototypes of devices, the Lloyd's mirror was used. For the fabrication of devices for actual use, the use of IL systems that can produce precise gratings is essential.

3.2.4 Measurement of Gratings

Fabrication of the gratings must be accurate to the period desired in order to control the center frequency of the reflected radiation. However, there is not much room for error. When compounded by the accuracy of an IL system's period control, we have to take into consideration the bounds of error. For the case of the Lloyd's mirror, the

rotation stage is only accurate to a degree. It must be kept in mind that the desired period of the gratings were calculated from the measurements of the refractive indices of the core and cladding as well as the thickness of those films. Reliability for those measurements is also vital. Figure 3.2.7 analyzes the bounds and limits of using any IL system for the 1530nm-1565nm band using a 325nm laser.

λ_0 (reflected center wavelength)	1530nm	1547.5nm	1565nm
n_{eff}	1.46483	1.4646	1.46445
Λ (grating period)	522.25nm	528.3nm	534.33nm
θ_{IL}	18.1288°	17.914°	17.7052°

Figure 3.2.7: Tolerances in grating period for λ_{IL} = 325nm and 3.36um core

It should be emphasized that the tight angular restrictions applies to all two-beam IL systems. To improve the tight angular restrictions of the beam angle, a longer IL beam wavelength can be used but would require a compatible ARC and photoresist. To increase the reliability of the Lloyd's mirror, a precise rotational stage would be required.

Next, we would like to measure the period of the gratings that we exposed. Most surface scanning metrology tools do not have the resolution required to measure periods with sub nanometer precision. The best tool to do the job is a scanning electron microscope (SEM) that has the ability to calibrate out any intra-field distortion that would otherwise introduce errors in measurements. The Raith 150, an SEM converted into an electron beam lithography tool, was used to take snapshots of several periods at once. From these snapshots, the average period was calculated. This allowed us to determine the drift in period that occurs when spherical wave fronts are used in IL systems [4].

Of course, the best way to determine the grating period is to fabricate a device with just a Bragg grating etched into the core. The transmission spectra would explicitly determine the period that was exposed.

3.2.5 Processing

The following is a step-by-step process of what was done for fabrication.

1. Spin on 211nm of Barli ARC at 2500 RPM

   The following is a spin curve for Barli ARC straight from the bottle

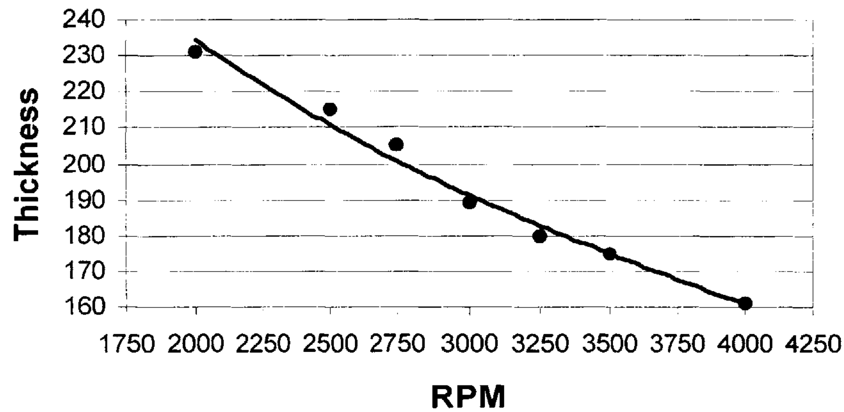

Figure 3.2.8: Barli ARC Spin Curve

2. Bake wafer on hotplate at 175°C for 1 minute
3. Evaporate 20nm of SiO_2 interlayer
4. Apply HMDS for 1 minute and spin dry off
5. Spin on 200nm of Sumitomo PFI-88 A3 positive photoresist at 8000RPM

   The following is a spin curve for PFI-88 A3 straight from the bottle

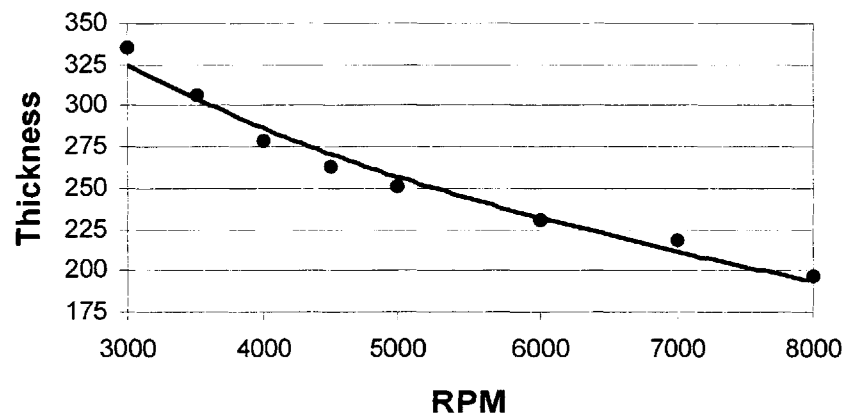

Figure 3.2.9: PFI-88A3 Spin Curve

6. Bake wafer at 90°C for 1 minute
7. Cleave wafer into quarters to maximize use of material
8. Align in Lloyd's mirror placing the quarter wafer edge to the mirror edge visually. Position quarter wafer so that the grating region starts slightly after mirror edge to minimize on chirp. Align the angle of the mirror to 234.25° assuming zero tilt is centered at 216.25°. This will shoot 528nm period gratings.
9. Expose in Lloyd's mirror for 5 minutes for 50% duty cycle provided that laser output is 52mW
10. Overlay grating region transparency mask and align to quarter wafer edge in the Tamarack. Transparency masks are positive film transfers with the emulsion on the back side.

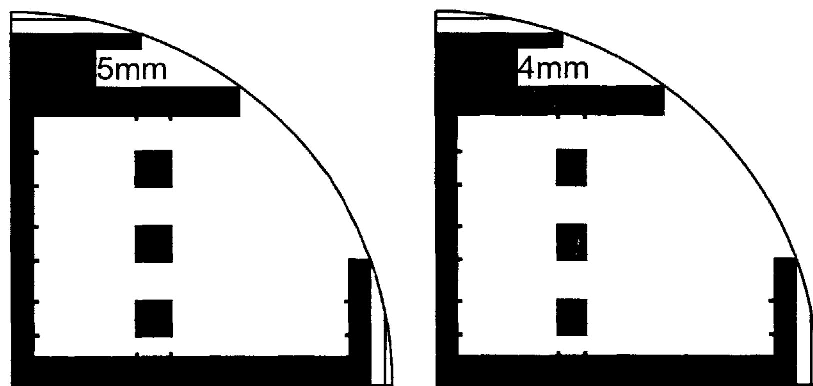

Figure 3.2.10: Grating Region Transparency Mask

11. UV flood expose quarter wafer for 25 seconds
12. Develop gratings in CD-26 positive photoresist developer for 60 seconds
13. Rinse in DI Water
14. Clear out any residual resist that may be left using the Plasmatherm RIE (descum). 20sccm O_2 and 4sccm He at 7mTorr with 250V DC Bias for 15 seconds.
15. Etch through 20nm of SiO_2 interlayer using the Plasmatherm RIE. 15sccm CHF_3 at 10mTorr with 300V DC Bias for 50 seconds
16. Etch through 211nm of ARC 20sccm O_2 and 4sccm He at 7mTorr with 250V DC Bias for 3 minutes
17. Evaporate 20nm of Cr to serve as the grating mask

18. Liftoff Cr in a Piranha clean (1:3 H_2O_2:H_2SO_4) for 5 minutes. Piranha clean also serves to clean surface for subsequent steps.
19. Rinse in DI water for 60 seconds

3.2.6 Summary

Using interference lithography is necessary for exposing large area gratings. These gratings serve to reflect a band of wavelengths whose center frequency is determined by the period of the gratings. Creating these gratings requires an IL scheme that can expose precise and accurate periods that are chirp-free. Measuring these devices required the use of an electron beam lithography tool due to its ability to calibrate out intra-field distortion.

3.3 Waveguide Hard-mask Definition

3.3.1 Couplers

Since Bragg gratings reflects bands of wavelengths in the reverse direction of propagation, there needs to be a way to separate the reflected signal from the incoming signal. Couplers are used to do such a task.

A coupler is a generic term for two waveguides that are brought close enough together so that power from one waveguide is transferred to another. This phenomenon occurs whenever the propagating mode profile intersects the area where a mode can exist in the neighboring waveguide. Since mode profiles in channel waveguides extend beyond the core into the cladding, controlling the distance between two waveguides will control the strength of the coupling. Once power has completely transferred to the neighboring waveguide, the power will transfer back [24]. Figure 3.3.1 depicts a coupler that is long enough to couple power fully to the other waveguide. Because of the symmetry, every input port can also be an output port and vice versa.

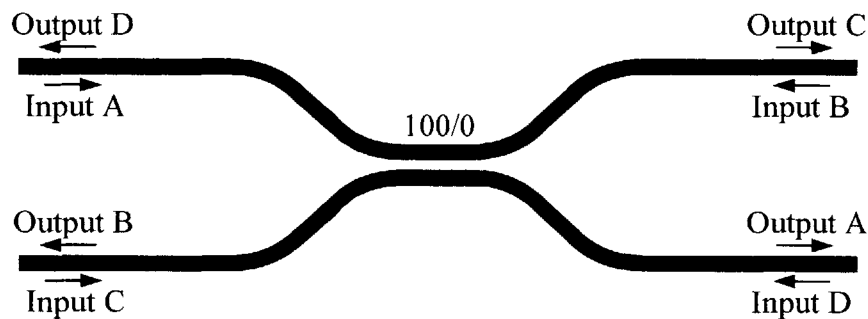

Figure 3.3.1: 100/0 symmetric coupler

Maxwell's equations state that two modes exist when two waveguides are close, a symmetric and an antisymmetric propagating mode. The symmetric mode occurs when equal power exists in both waveguides and no net power transfer occurs. The antisymmetric mode occurs when power is transferred from one waveguide to the other. Antisymmetric modes always propagate slightly slower than symmetric modes.

Subtracting the difference in propagation constants yields the coupling constant for a given distance [25].

In order to determine the length of the coupled region and how far apart the waveguides should be, calculation of a coupling constant for various waveguide distances must be done and an exponential fit made [19]. As the waveguides gradually approach and deviate towards the coupling region, integration can be done to determine the total coupling. Because propagation constants have units in radians per meter, the coupling constant will represent total phase shift per meter, or in other words, how much power is transferred to the other waveguide for a given length.

For the case of the add/drop channel filter, we require the use of 50/50 power splitting couplers. Implementing a 50/50 coupler in front of the grating region will require two identical gratings on both arms which will then reflect back to the coupler and complete the 50/50 power transfer to the drop port. Figure 3.3.2 shows what happens.

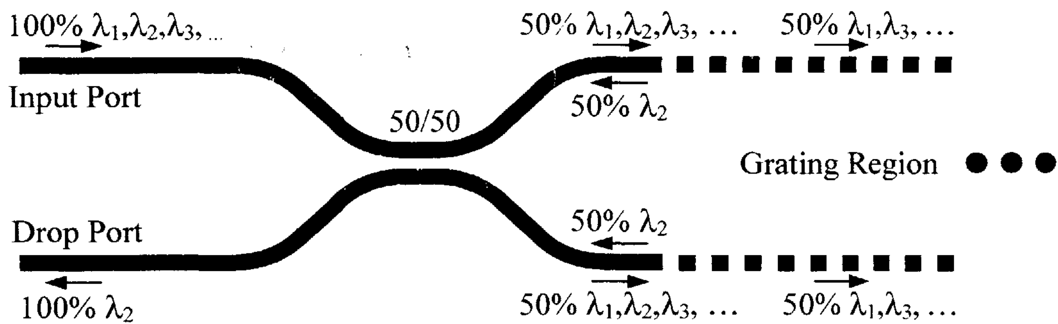

Figure 3.3.2: 50/50 Coupler in Front of Grating Reflecting λ_2

This figure over simplifies what is actually happening. This form of coupler is only perfectly 50% power splitting at one wavelength. Using cascading couplers can provide wavelength insensitive couplers [26].

3.3.2 Bends

Waveguides are able to confine light and guide it to a particular destination. However, if the waveguide is bent too much, or if there are surface imperfections in the core, the conditions for total internal reflection can be violated and light would scatter out

of the waveguide into the cladding resulting in transmission power loss. Figure 3.3.3 shows a ray diagram of two types of scattering loss mechanisms [20].

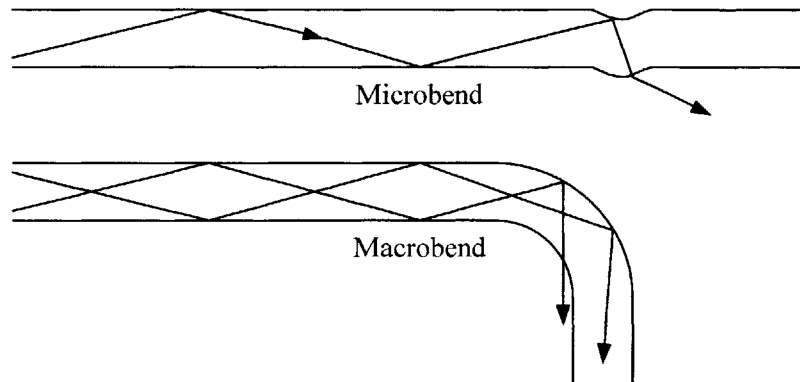

Figure 3.3.3: Loss by bends

To control microbends in the core, effort must be given to ensure the four sides of the core are smooth. CMP, described in Section 3.1.4, and sidewall roughness control during the waveguide patterning must be used.

To minimize loss due to macrobend scattering, the radius of curvature used in the couplers would be very large. However, loss due to the oxynitride core must be considered. The longer the waveguide is, the more loss contributed by the material. The smaller the radius of curvature is, the more loss contributed from scattering. There are several ways of calculating scattering loss versus radius of curvature [19,27,28]. Most methods start of simplifying the problem by using conformal transformation to convert the bend into a straight slab waveguide and changing the refractive index profile accordingly. Figure 3.3.4 describes the bending loss while choosing 0.1dB/cm to be the maximum tolerable scattering loss.

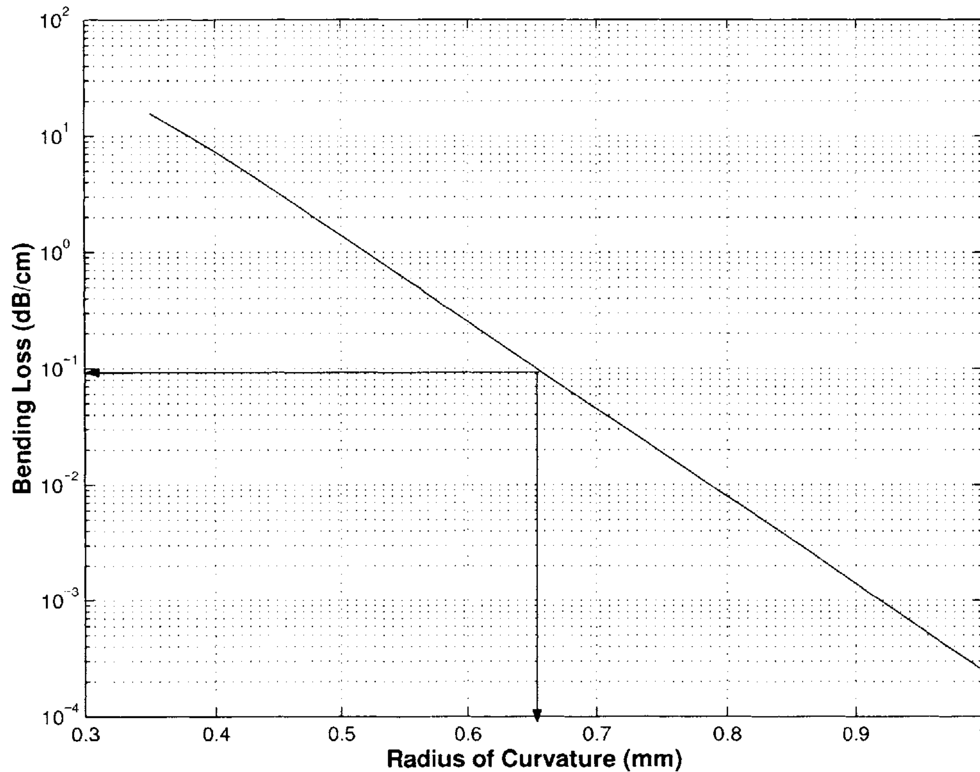

Figure 3.3.4: Bending loss vs. Radius of Curvature for a 3.44um core

3.3.3 Waveguide Pattern Generation

To define the waveguide patterns and aligning them to the gratings, electron beam lithography (EBL) was used. EBL allows the prototyping of many different devices without the added step and cost of creating masks. However, EBL is expensive to purchase and requires an operator who knows the tool well. Luckily, an EBL tool and knowledgeable people are present at NSL. The tool used is the Raith 150, a converted SEM marketed for universities and small companies interested in prototyping and research.

This means that the price of the Raith is much lower than higher end EBL systems. This also means that there are many quirks with the system in hardware as well as in software. Characterization of the tool is a constant ongoing affair as different patterns and substrates are used challenging the potential of the system.

The Raith 150 has support for various input formats for pattern definition. It also has the ability to take in text input to specify boxes, polygons, and paths. Although paths may

appear to be the natural choice for waveguides to be defined, the Raith software generates errors for particular structures, the nature of which is still unknown. Thus, polygons, which define the outline of structures, were generated point by point using MATLAB. Because of the desire to keep microbends at a minimum in the curved coupler regions, many points were used. However, the Raith only supports polygon structures with a maximum of 1024 points. Therefore, the MATLAB code must split the waveguide into segments with 1024 or fewer points each.

To define the structures, only 7 variables are needed. The minimum distance between two couplers, the maximum distance, radius of curvature, arc length of curves, length of parallel coupled region, length of the grating region, and the thickness of the waveguide. Figure 3.3.5 shows the placement of the variables specific for just the coupling region. Figure 3.3.6 shows a MATLAB depiction of a just the coupler. Note the scale differences in the y direction.

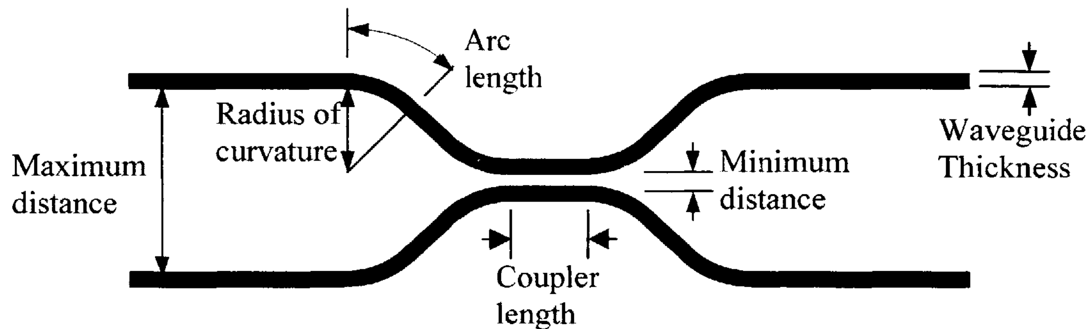

Figure 3.3.5: Variables that Define a Coupler

3.3.4 Measurement of Line Profiles and Widths and Dynamic Deflection

The Raith 150 came pre-configured to operate with an acceleration voltage of 5kV. However, to expose thicker resists evenly, higher acceleration voltages are needed. We are interested in using 200nm of PMMA because of the necessity for 85nm of material to be lifted off to withstand the long subsequent etches which will be described in Section 3.4. Settling upon a higher acceleration voltage of 20kV, characterization of several parameters has to done to ensure optimum results.

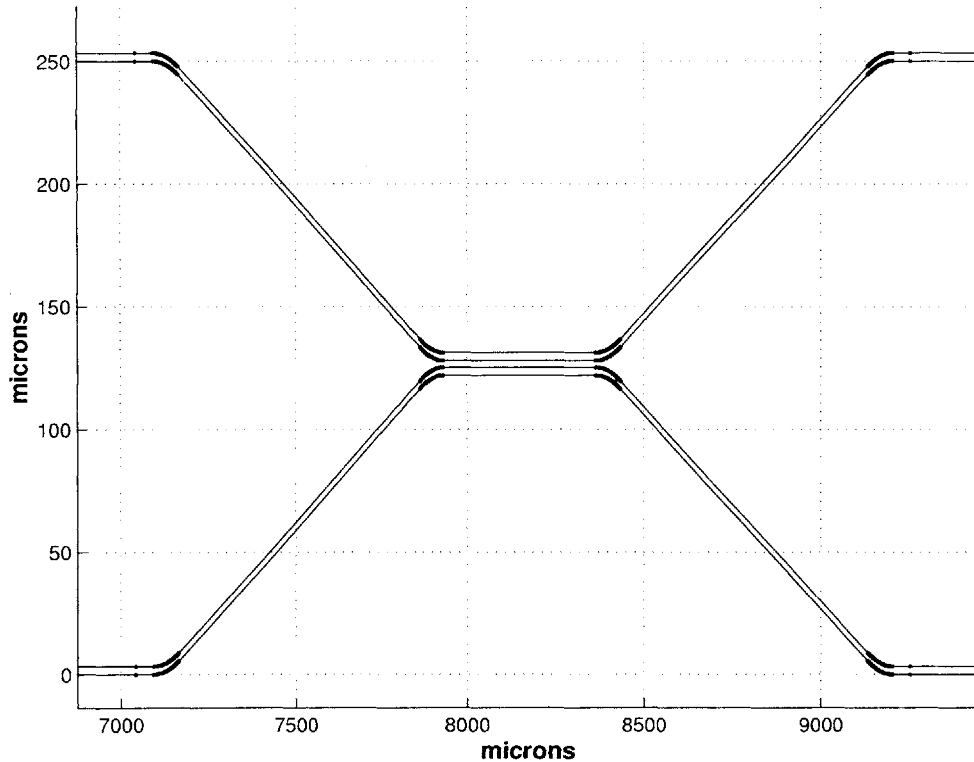

Figure 3.3.6: MATLAB representation of coupler

Two main parameters that need to be tweaked before pattern placement are the exposure dose and line width biasing. The exposure dose is the amount of charge that is aimed at a unit of area. If the amount is not enough, the sidewall profile of the line would not be straight, causing underexposed sidewalls. If it is too much, the line width would expand in size due to the profile of the electron beam. Straight sidewalls and a slight undercut at the base of the resist is optimal for liftoff. Undercut is caused by slight back scattering off the material directly underneath the resist exposing the area underneath the sidewall [22].

Underexposed sidewalls are undesirable for the liftoff of material since material may be peeled away. Figure 3.3.7 shows underdosed versus a good exposure.

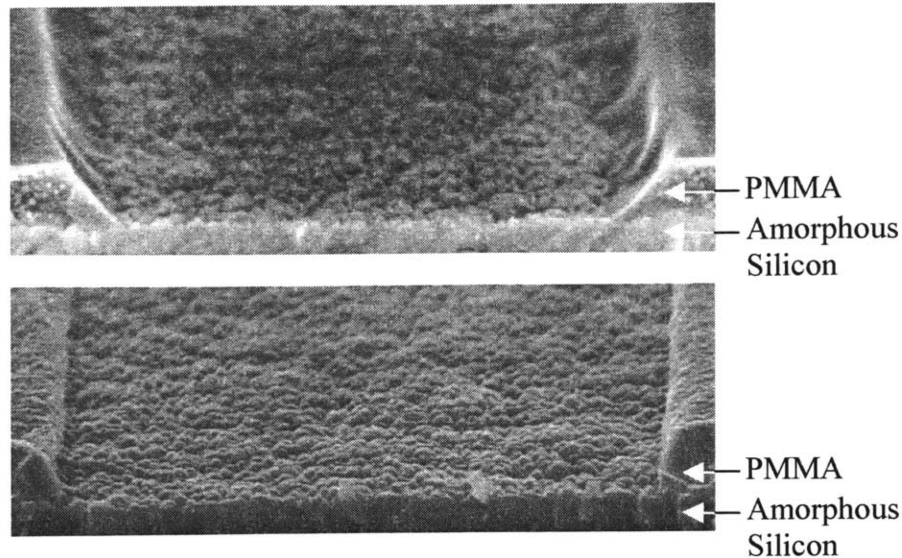

Figure 3.3.7: Underexposed (top) vs. good exposure (bottom) for 2.7um linewidths

Line width biasing is determined after the exposure dose is decided upon. The line width is usually larger than expected, mostly due to the over exposure required to produce an undercut as well as the Gaussian profile of the electron beam. Since the Raith 150 has the ability to do intra-field calibration, measurement of line widths are done to determine the biasing that needs to be set during the MATLAB generation of the waveguide pattern.

An additional parameter to find is the dynamic deflection correction. The way the Raith 150 writes lines is by first blanking the beam, preparing the deflection coils to start behind the beginning of a line, taking a running start, and then unblanking the beam at the right time. Figure 3.3.8 and 3.3.9 shows when the timing of the unblanking of the beam goes awry.

There are two ways of correcting for dynamic deflection. One is to change the system parameters and the other is to modify the MATLAB waveguide pattern to overlap the boundaries to compensate. Figure 3.3.10 shows when the latter was done when the pattern segments overlap too much resulting in overexposed regions. Figure 3.3.11 shows the parameters that provide undercut, line width control, and dynamic deflection correction for 20kV acceleration voltage.

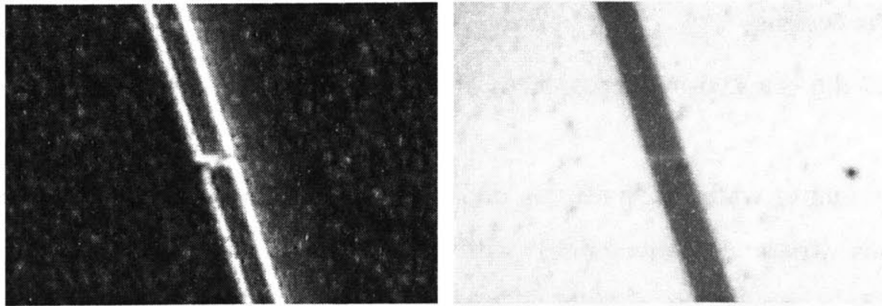

Figure 3.3.8: Dynamic Deflection. Optical micrograph of PMMA (left) and SiO_2 (right)

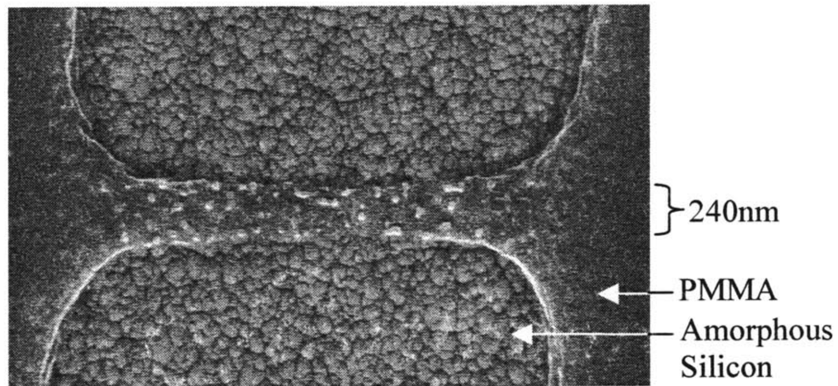

Figure 3.3.9: Dynamic Deflection Error. SEM of boundary

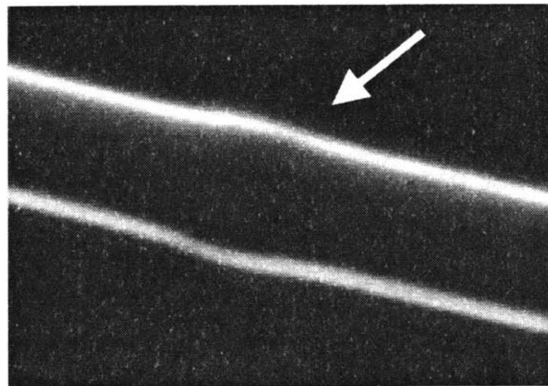

Figure 3.3.10: Overexposure from Pattern Segment Overlap

Dose ($\mu C/mm^2$)	Line width Bias	Overlap
180	-40 nm	180 nm
195	-90 nm	150 nm
210	-140 nm	120 nm

Figure 3.3.11: Dosage, Line Width Bias, Overlap for 20kV Acceleration Voltage

3.3.5 Processing

The following is a step-by-step process of what was done for fabrication.

1. Place quarter wafer in sputtering deposition system and place scrap silicon on top in regions where no waveguides will be patterned. Leaving gratings exposed will provide a means for angular alignment to the gratings as well as the ability to determine relative position to the grating regions.
2. Sputter 520nm of Silicon at 200W with 25sccm Ar flow. 1 hour of deposition will achieve this thickness.
3. Spin on 200nm of 3.5% PMMA on top of the amorphous silicon @ 4500RPM
4. Evaporate 5nm of Cr to provide a conductive layer to prevent charging during electron beam lithography.
5. Place quarter wafer in the Raith 150 and calibrate the writing field axes to the exposed grating region.
6. Direct write waveguide pattern
7. Wet Etch Cr completely away in CR-7 Chromium Etchant for 15 seconds
8. Develop PMMA in 1:2 MIBK:IPA at 21°C for 1 minute.
9. Rinse in IPA for 1 minute to kill the developing.

3.3.6 Summary

To define the waveguide pattern, calculations must be made to determine the radius of curvature for the couplers to minimize on transmission loss.

MATLAB was used to generate the waveguide structures point by point. A text file with the points was given to the Raith 150, an electron beam lithography tool. Exposure dose, line width biasing and dynamic deflection correction parameters were determined to expose the waveguide pattern in PMMA.

3.4 Etching of Waveguides and Gratings

3.4.1 Waveguide Hard-mask Dry Etching

After patterning the gratings in PMMA, it is time to transfer the pattern into the amorphous silicon hard-mask. To do so, a protective layer is needed to protect the amorphous silicon where the waveguides will be. This amorphous silicon layer will serve as a hard-mask for the subsequent oxynitride etching which ultimately defines the waveguide structure. However, there also exists a chromium grating hard-mask underneath the amorphous silicon that needs to be cleared before the waveguide can be etched.

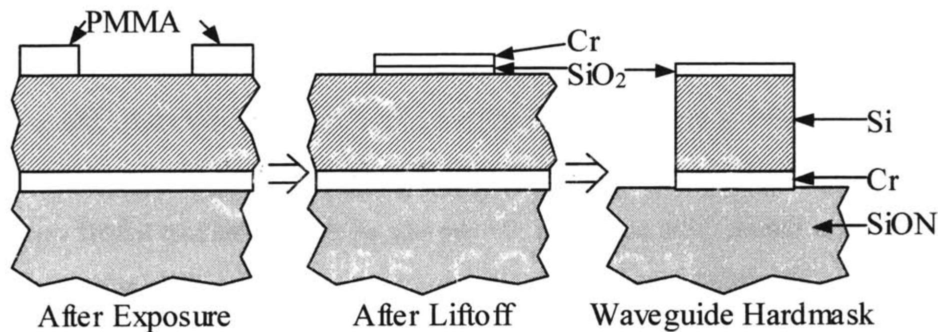

Figure 3.4.1: Waveguide Hard-mask Dry Etching

To etch the amorphous silicon, a Cl_2 atmosphere is used. The mask needed to form the amorphous silicon hard-mask is SiO_2. It provides excellent etch selectivity towards silicon in chlorine, greater than 10:1 for $Si:SiO_2$. However, an additional thin layer of chromium is also needed to protect the amorphous silicon from the aggressive chromium etching that follows.

The chromium grating hard-mask, which resides underneath the amorphous silicon, needs to be cleared from everywhere except from underneath the waveguides. To recapitulate, the chromium grating serves to pattern the Bragg gratings on top of the oxynitride core. Because chromium is present everywhere, wet etching chromium would

yield uneven etching across the whole quarter wafer and would undercut underneath the amorphous silicon as depicted in Figure 3.4.2.

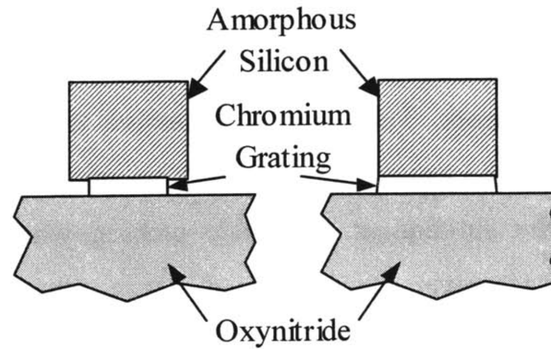

Figure 3.4.2: Chromium Wet Etch Undercut (left), Dry Etch (right)

Thus, dry etching the chromium is desirable. However, there are two drawbacks to dry etching using reactive ion etching. One is how vertical the sidewall of the chromium mask can be. The other is the aggressive nature of a chromium dry etch. The presence of oxygen as well as the high pressures and high RF power required also etches away the amorphous silicon faster. This accounts for the use of the chromium liftoff on top of the silicon dioxide mask which is protecting the amorphous silicon. This will guarantee the amorphous silicon will survive the chromium etch. It should be noted that the additional chromium liftoff can be substituted for a thicker amorphous silicon layer. Figure 3.4.3 shows the difference using the chromium liftoff protective layer for the same thickness of SiO_2 mask and amorphous silicon.

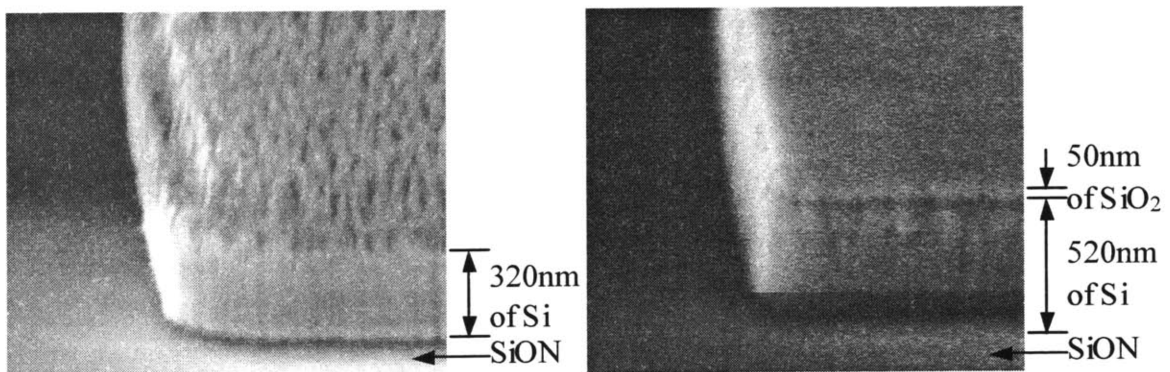

Figure 3.4.3: Without (left) vs. With (right) Cr liftoff after Cr Dry Etch

Chromium dry etching is typically used for patterning features on photolithography masks, field emission display gate electrodes, and thin film transistor liquid crystal displays. The etch chemistry involved is Cl_2 and O_2. Increasing the O_2/Cl_2 flow ratio increases the etch rate of chromium both vertically and laterally [29]. However, the vertical etch rate is typically three times greater than the lateral etch, forming sloped sidewalls. Using lower pressures and higher DC biases can help in straighter sidewalls.

A Perkin & Elmer RIE, a converted sputter deposition system, was used for the amorphous silicon and chromium etching. It was found that to have reasonable rates of chromium etching, high pressures and high plasma wattages were required. The etch selectivity between amorphous silicon and chromium was 10:1 at a pressure of 65mTorr and 200W power (450V DC Bias) using 40sccm of Cl_2 and 10sccm of O_2. Etch rates were a modest 40nm per minute.

3.4.2 Oxynitride Dry Etching

After exposing the oxynitride underneath the chromium hard-mask, we are now ready to do a deep oxynitride etch to define the waveguide structure. Figure 3.4.4 depicts the process steps.

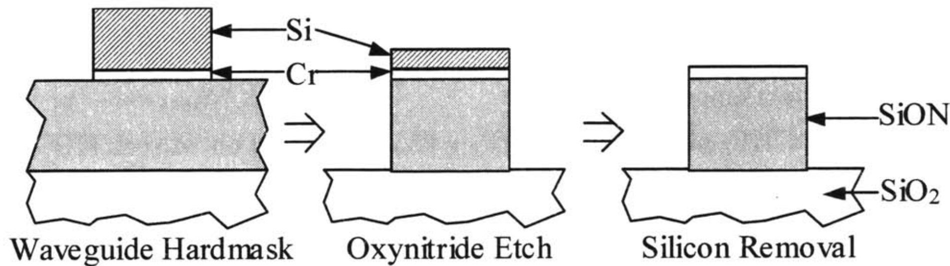

Figure 3.4.4: Oxynitride Waveguide Etching

Two reactive ion etchers were considered for the deep oxynitride etch for the waveguides, a Plasmatherm and a March CS-1701. The Plasmatherm has excellent repeatability and is well maintained; however, deep oxynitride etches aren't considered to be an acceptable process for the tool due to the long etch times and clean cycles. It is capable of locking either the DC Bias voltage or the RF wattage during an etch. The March RIE is dedicated for long etches of organic materials as well as nitrides and

oxides; however, the tool was not setup to display the DC Bias voltage. Repeatability for the March is moderate and is highly dependent on what was etched prior, regardless of whether the chamber was cleaned. However, the advantage the March has is its ability to etch at high pressures theoretically yielding higher etch rates. Surprisingly, when operating at peak performance, both RIE tools have similar etch rates.

Two etch chemistries were also used: CHF_3 versus CHF_3+O_2. CHF_3 is known for its sidewall passivation allowing for high aspect ratio etches. However, CHF_3 with O_2 has straighter sidewalls than CHF_3 alone. Figure 3.4.5 shows a 3.44um deep etch using 400W at 125mTorr on the March RIE with no oxygen and introducing oxygen.

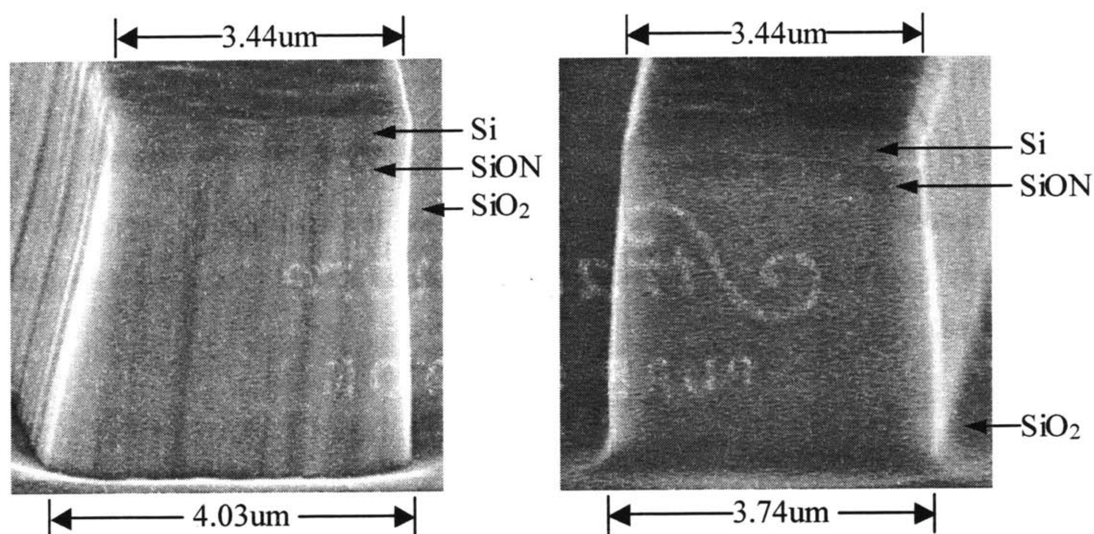

Figure 3.4.5: CHF_3 alone (left), CHF_3 + 6% O_2 (right) on March RIE

The presence of oxygen helps attack the sidewall passivation allowing for straighter sidewalls, but at the expense of shorter lifespan of the amorphous silicon hard-mask. Comparing the etch rate ratios of oxynitride to amorphous silicon, CHF_3 alone gives a selectivity of 10:1 while CHF_3 with 6% O_2 only gives 2.5:1.

To improve the sidewall profile, lower pressure and higher DC Bias is required. Using the Plasmatherm with a flow rate of 20sccm of CHF_3 at 10mTorr with a DC Bias of 350V, an etch rate of 41.7nm/min at 350W power was achieved. For the March RIE, similar etch rates were achieved, but was unpredictable due to the inability to control and view the DC Bias.

Figure 3.4.6 shows an SEM micrograph of a deep oxynitride etch. Notice the chromium gratings that have not been completely cleared from the chromium dry etch process and how their profile transfers down the side of the waveguide.

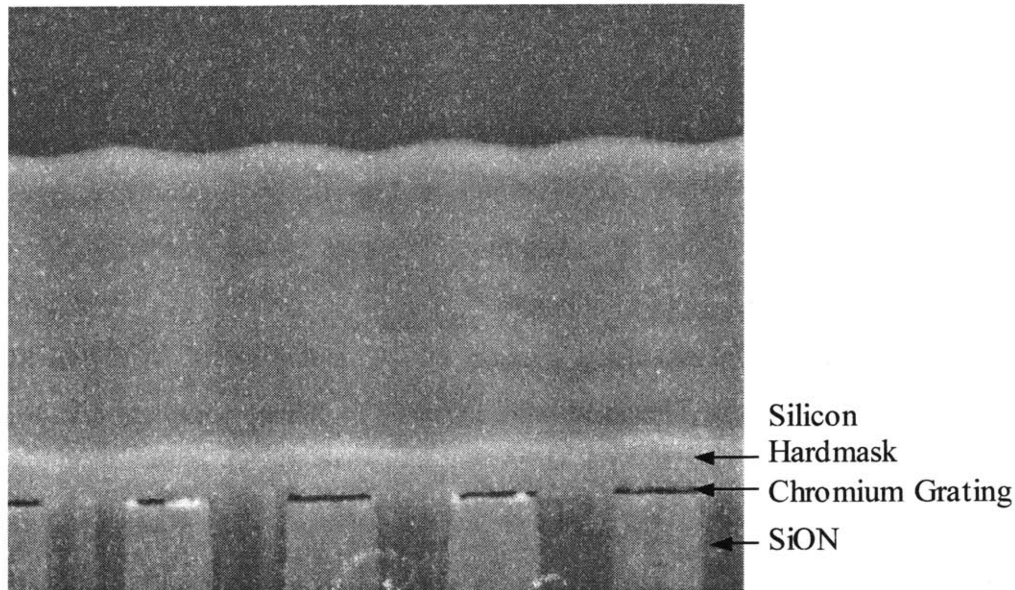

Figure 3.4.6: After Deep Oxynitride Waveguide Etch

3.4.3 Processing

The following is a step-by-step process of what was done for fabrication.

1. UV Ozone clean the pattern to ensure good liftoff
2. Evaporate 70nm of SiO_2 (mask for chromium etch) and 15nm of Cr (to protect SiO_2 from long silicon etch)
3. Liftoff PMMA by dissolving in hot NMP at 110°C for 10 minutes while shaking gently. Spray with NMP while pulling out of solution to ensure PMMA is washed off
4. Rinse with acetone for 1 minute before the NMP dries.
5. Using the Perkin & Elmer RIE (a converted sputtering deposition system), do a descum etch using 15sccm O_2 and 30sccm CHF_3 at 50W (400W DC Bias) at 15mTorr for 15 seconds to clear off any organics and thin oxidation layers that may have formed on the amorphous silicon surface.

6. Etch amorphous silicon using 40sccm of Cl_2 at 50W (425W DC Bias) at 15mTorr for 5.5 minutes. This is actually an overetch to ensure complete removal of unwanted silicon. Overetching would slightly etch any oxynitride exposed through the chromium grating hard-mask. This is not a concern since the subsequent deep oxynitride etch would average the grating pattern away. At this point, any chromium that was exposed before etching would be gone revealing only the chromium hard-mask that was underneath the amorphous silicon.
7. Perform an etch using 30sccm of O2 at 50W at 15mTorr for 2 minutes to remove any organics and to pre-oxidize the chromium to assist in the following dry etch of chromium.
8. Etch chromium hard-mask using 40sccm of Cl2 and 10sccm of O2 at 200W at 65mTorr for 45 seconds. This is another overetch to ensure complete removal of the chromium.
9. The quarter wafer is now ready for the deep oxynitride etch. Keep in mind that a subsequent grating etch will be done so subtract the desired waveguide height by the grating height. Using the Plasmatherm, etch in 20 minute cycles, using 20sccm of CHF_3 at 350V DC Bias at 10mTorr. After each cycle, take out the quarter wafer and do a clean run using 20sccm O_2 and 4sccm CF_4 at 350V DC Bias at 20mtorr for 15 minutes. Etch rates will vary depending on the cleanliness of the chamber and the power entering the plasma. Using the Dektak profilometer, measure the height of the waveguides to determine the etch rates. Figure 3.4.7 shows etch rates vs. plasma power at 350V DC Bias.

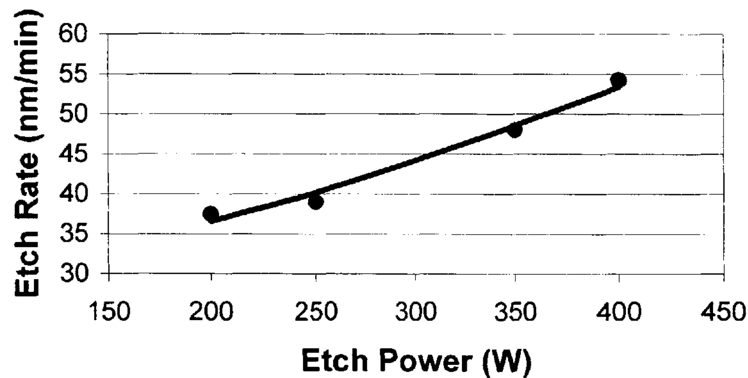

Figure 3.4.7: Etch Power vs. Etch Rate on the Plasmatherm at 350V DC Bias

10. At this point, we want to remove the amorphous silicon hard-mask layer that still resides. Examine how much silicon is left in an SEM. Make sure no gold/palladium is deposited.
11. The amorphous silicon hard-mask now is covered by a passivation polymer deposited from the CHF_3 etch. Placing the quarter wafer back into the Perkin & Elmer RIE, use 30sccm of O_2 at 50W at 15mTorr for 2 minutes followed by 30sccm of CF_4 at 50W at 15mTorr for 15 seconds.
12. Etch away the amorphous silicon hard-mask layer in 40sccm of Cl_2 at 50W at 15mTorr. Etch rates for silicon is about 70nm/min. But it is recommended to overetch slightly to ensure complete removal of the amorphous silicon hard-mask.
13. Place the quarter wafer back into the Plasmatherm and proceed to etch the gratings using the chromium that was under the amorphous silicon as a hard-mask. Depending on what grating etch depths were chosen in Section 3.2.1, and using the etch rates determined earlier, etch using 20sccm of CHF_3 at 350W at 10mTorr.
14. Perform a descum etch, 20sccm of O_2 and 4sccm of CF_4 for 2 minutes to clear out any passivation material deposited on the chromium hard-mask as well as oxidize the chromium to prepare for removal.
15. Wet etch chromium in CR-7 chromium etchant for 2 minutes to ensure complete removal of the chromium.

3.4.4 Summary

Cr and SiO_2 were used to protect the underlying amorphous silicon waveguide hard-mask from a long silicon etch and an aggressive chromium etch respectively.

Etching through microns of oxynitride requires several cycles with clean runs in between to ensure the chamber of the RIE being used does not revert from etching to depositing material on the chamber walls of the device.

Removal of the silicon hard-mask and chromium hard-masks both require descum etches to remove organic buildup and passivation polymers that form during etching of other materials.

Close attention to DC bias and power wattage can predict etch rates during etching. Low wattages signal or weak and flickering plasmas signal the need to do a clean run or scrub down the chamber of the RIE.

3.5 Top Cladding Deposition

3.5.1 ECR Plasma Enhanced Chemical Vapor Deposition

At this point, all there needs to be done is to deposit an upper cladding of silicon dioxide. There exists a multitude of methods to do such a task, but only one method was available and accessible. Because the Novellus Concept-One does not allow any samples exposed with gold, another tool manufactured by Plasmaquest was used. This tool incorporates Electron Cyclotron Resonance (ECR) to a PECVD system. The difference between the Plasmaquest and the Novellus Concept-One is in the generation of a high-density plasma. The plasma is generated by coupling microwave energy with the natural resonant frequency of the electron gas in the presence of a powerful static magnetic field. ECR generates a high degree of ionization, can deposit and etch films at relatively high pressures (10^{-4}-10^{-3} Torr) and at low temperatures (<200°C) [31]. In fact, the Plasmaquest can deposit silicon dioxide films at pressures higher than 40mTorr and at temperatures as low as 40°C.

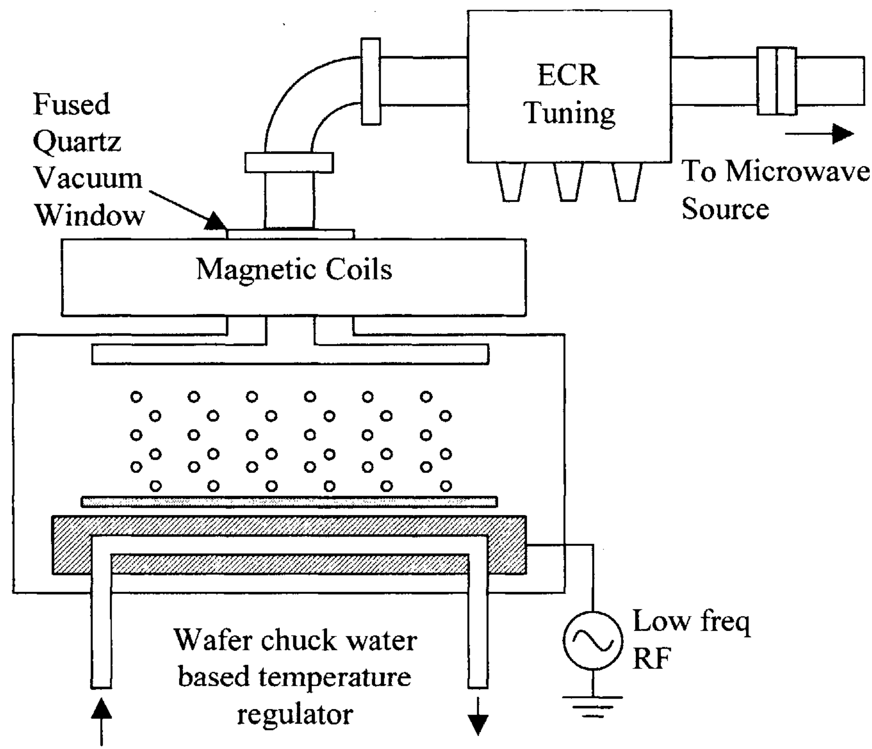

Figure 3.5.1: Diagram of Plasmaquest ECR PECVD

To deposit silicon dioxide films, the Plasmaquest uses gas flows of SiH_4 and O_2. It was noted in Section 3.1.2 that this atmosphere is considerably more reactive yielding worse uniformity and more particle contamination than SiH_4-N_2O films. However, that was for RF based plasmas. ECR plasmas are considered to be more efficient at creating plasmas and preventing particles from forming in the atmosphere before they touch the substrate. However, too much or too little ECR wattage can yield poor film quality in terms of cohesion, adhesion, and the film content.

The drawbacks to using the Plasmaquest are that the tool is also used for etching almost everything imaginable and maintenance of the tool is poor. The hours of availability are few due to the high demand for the tool as well as the shut down of toxic gas flows after hours.

3.5.2 Conformal Deposition

Depositing the top cladding is not the same as depositing the lower cladding. With the lower cladding, only a planar film was needed and a flat wafer was provided. For the top cladding, silicon dioxide needs to fill in the trenches in between the grating teeth as well as along the sides of the waveguide. To do so, we take advantage of the secondary RF source that the Plasmaquest has located on the wafer chuck. This RF source oscillates at a much lower frequency than the ECR source and provides the same benefits as the low frequency RF source in the Novellus Concept-One. As stated before, this low frequency RF source provides increased conformity and reduction of stress of the deposited film.

The increased conformity comes from a phenomenon called "resputtering". When the substrate RF bias is introduced, ion bombardment is induced towards the substrate that may lead to re-sputtering, knocking loose deposited material which is redeposited nearby [16]. This leads to enhanced surface mobility that yields better topographical control and step coverage. The ions in this case are Si, O, and H. Introduction of an inert gas can be used to promote resputtering [32].

Figure 3.5.2 shows the mechanism behind resputtering. Ions formed by the plasma are directed towards the substrate and interact in a variety of ways. They can deposit and form any combination of bonds associated with PECVD SiO_2 films. The ions can knock loose deposited material that may redeposit or the loose material can become reionized.

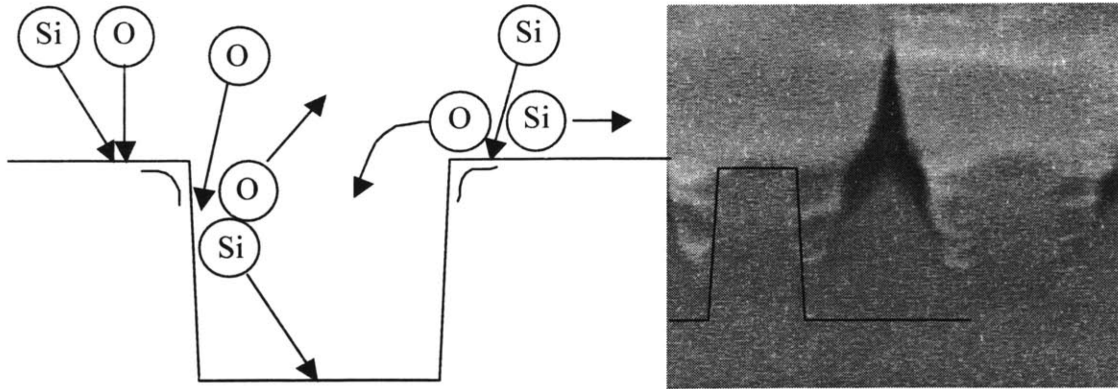

Figure 3.5.2: Generalized surface processes in PECVD resputtering

Close attention should be paid to the case when deposited material is sputtered off the substrate. As the substrate RF bias is increased, the refractive index of the film increases indicating the lower oxygen content and presence of more Si—Si bonds. This is an indication of the oxygen being sputtered away and silicon filling in the grooves. Figure 3.5.3 shows an SEM cross-section of a grating that has been deposited upon at the highest substrate bias possible. An HF dip was made and the result shows that the oxynitride material from the Concept-One etched very quickly while the top cladding resisted due to the high silicon content. Figure 3.5.4 shows the effect of increasing the substrate bias on the filling of grooves.

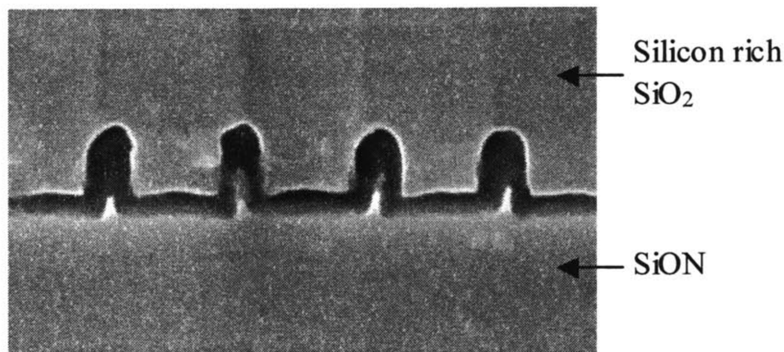

Figure 3.5.3: HF Dip of Silicon Rich Top Cladding on SiON

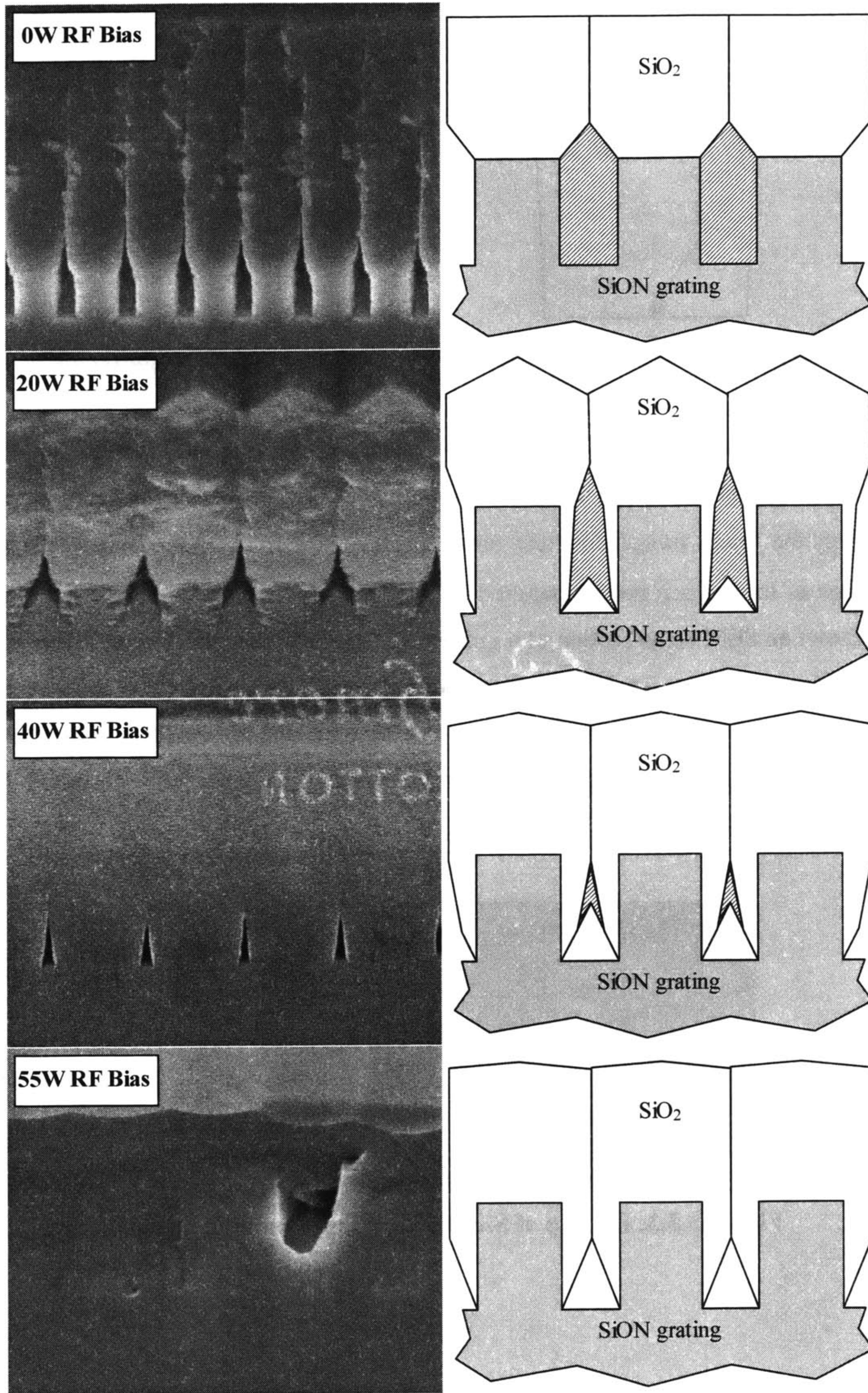

Figure 3.5.4: Increasing Substrate Bias for Conformal Deposition

Because of the high-energy ion bombardment, resputtering can significantly lower the net deposition rate. However, if the net deposition rate deposits the film too fast, resputtering would not have enough time to fill in the voids. In fact, if the RF substrate bias is not set high enough, the incident angle at which the ions impinge the surface may cause faceting, creating voids that can't be filled by resputtering [30].

There is also the danger of damaging the material that is being deposited on. The regions that are in most danger to ion bombardment are the corners of the gratings. To solve this problem, a pre-deposition is done with zero RF bias. With a layer of oxide for protection, the RF bias is turned on.

It should be noted that ECR PECVD does provide a benefit to resputtering. Because of the higher density of ions that is generated by ECR, higher aspect ratio trenches can be filled than without ECR. Typically, without ECR, a maximum of 1.0 aspect ratio is achievable. To do more, ECR is needed [32].

3.5.3 Measurement of Thin Films

Utilizing the substrate RF bias, conformal deposition can avoid the formation of voids. However, introducing the RF bias causes the refractive index to increase well beyond that of the core (indices were measured up to 1.7). Because of the resputtering ionization of the atmosphere, changing gas flows showed illogical effects on the refractive index. At times, increasing the oxygen flow would increase the refractive index when the reverse was expected. This has much to do with the oxygen being a catalyst for the resputtering effect.

To compensate for void formations, a decrease in SiH_4 flow was necessary in order to reduce the deposition rate and give resputtering time to work. If the deposition rate is lowered even more, lower RF bias voltages were needed. In turn, the refractive index decreases.

The following are recipes used as well as the refractive index and deposition rates measured using the Metricon. It has been found that pressure has little effect, if any, on the refractive index of the film or the ability to fill in voids.

SiH_4 (sccm)	O_2 (sccm)	Other (sccm)	Pressure (mTorr)	RF Bias	Refractive Index	Deposition Rate (nm/min)
90	21	4 He	40	20	1.4463	27.9
90	21	4 He	40	0	1.4366	28.2
90	23	4 He	40	0	1.4302	30.3
76	20	-	40	0	1.4420	22.5
78	18	4 He	40	0	1.4475	22.0
80	16	4 He	40	0	1.4388	28.3

Figure 3.5.5: Plasmaquest Recipes and Measurements

3.5.4 Processing

The following is a step-by-step process of what was done for fabrication.

1. Set the water chiller for the Plasmaquest to 85°C
2. One the Plasmaquest, deposit on the quarter wafer the desired recipe. Perform an aggressive clean etch for 20 minutes after every hour of deposition. The clean etch used was 20sccm of CF_4, 20sccm of SF_6 and 30sccm of O_2 at 80mTorr using 400W of ECR and 0W RF.
3. Densify in annealing tube at 1100°C for 3 hours (30 minute ramp up, 90 minute bake, 1 hour cool down)

3.5.5 Summary

Work previously done fabricating these devices utilized incremental PECVD TEOS depositions and annealing steps to avoid creating voids when filling in the grating regions. This form of deposition is very time consuming and harmful on the gratings in the core due to the constant exposure to high temperature annealing.

Resputtering allows for a means to fill in gratings without the need to anneal constantly. With the use of ECR PECVD, low temperature depositions can be employed with little risk of melting the grating regions. The downside to resputtering is its tendency to increase the refractive index of the film due to the loss of oxygen through being sputtered away. Much time must be taken to characterize the effect gas flows and RF bias have to film properties.

To find the tradeoff between deposition time and resputtering to avoid voids while keeping tabs on the refractive index is a huge undertaking. Fortunately, once a recipe has been found, the Plasmaquest is highly repeatable for depositions. Because sputtering is taking place, a predeposition with no bias is required to avoid sputtering of the core material.

Chapter 4
Conclusion and Future Work

A new material system using silicon oxynitride was implemented to solve the problem of the melting of the Bragg gratings due to the high temperature deposition of the top cladding [4]. In order to use this new material, a means to deposit the films as well as a means of characterizing their properties were developed. This included the use of PECVD and the Metricon. The melting of the gratings was no longer a problem due to the material change, as well as low temperature deposition using ECR PECVD.

However, the device has not gone through all the process steps perfectly. Figure 4.1 depicts a grating that was etched too deep because the amorphous silicon hard-mask did not last as long as expected. This was due to the aggressive chromium etching that etched away the silicon mask as well. The addition of the chromium layer on top of the silicon dioxide successfully protected the silicon mask through the silicon and chromium etches.

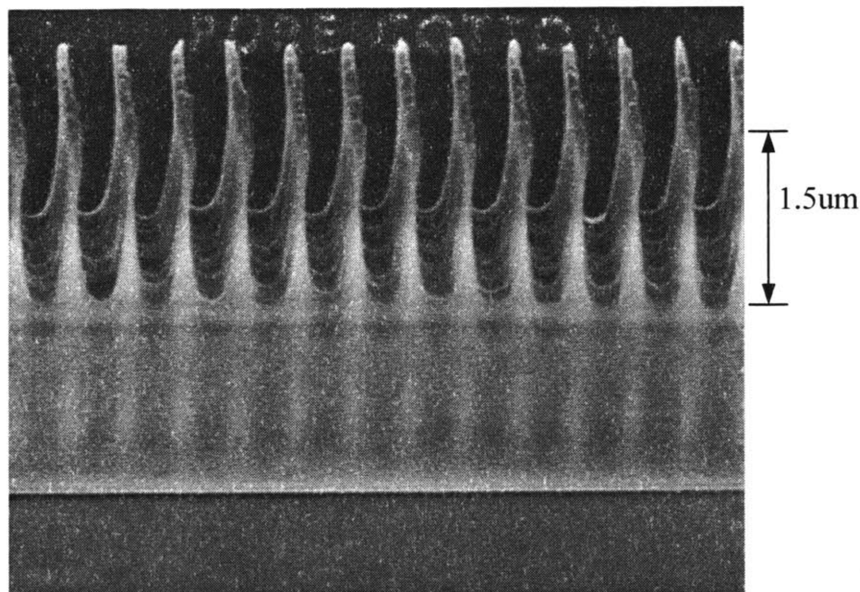

Figure 4.1: Over Etching of Gratings

But, as was shown in Figure 3.4.6, the silicon hard-mask was very stubborn and was very difficult to remove. The steps described in Section 3.4.3 to remove the silicon hard-mask have not been carried out. Instead, a wet-etch in hot TMAH at 80°C for 5 minutes was attempted to remove the silicon mask, but it had some film protecting it. Section 3.4 describes steps that would break away the film using a descum and dry etch away the silicon in a chlorine atmosphere. This would remove the film as well as remove the silicon as well as avoid the use of TMAH.

Another aspect that should be investigated is the refractive index of the Plasmaquest ECR PECVD RF bias resputtered depositions. A complete characterization of the refractive index versus various gas flows and RF biases would give a deeper understanding to the effect resputtering has on refractive indices, as well as how much RF bias is needed to maintain high aspect ratio trench filling.

It is to my regret that I could not have spent more time to fully answer these questions; however, it provides a challenging task to whoever wishes to follow. Much work still has yet to be done and further modifications to the design of the add/drop channel filter can be made to introduce tunability as well as switching capabilities. What can be done is left to the imagination.

References

[1] Rajiv Ramaswami, Kumar N. Sivarajan. *Optical Networks: A Practical Perspective, Second Edition.* Academic Press, San Diego, CA, 2002.

[2] Michael H. Lim, T.E. Murphy, J. Ferrera, J. N. Damask, and Henry I. Smith. Fabrication techniques for grating-based optical devices. *Journal of Vacuum Science and Technology B*. vol. 17, issue 6, pp. 3208-3211, 1999.

[3] Amnon Yariv. *Optical Electronics, Fourth Edition.* Saunders College Publishing, Philadelphia, PA, 1991.

[4] Thomas E. Murphy. *Design, Fabrication and Measurement of Integrated Bragg Grating Optical Filters*. PhD Thesis, MIT.

[5] Michael H. Lim. *Development of X-ray Lithography and Nanofabrication Techniques for III-V Optical Devices*. PhD Thesis, MIT, 2001.

[6] David K. Cheng, *Fundamentals of Engineering Electromagnetics*. Addison-Wesley Publishing Company, Reading, MA, 1993

[7] Jin Au Kong. *Electromagnetic Wave Theory*. EMW Publishing, Cambridge, MA, 2000.

[8] G. R. Hadley and R. E. Smith. Full-Vector Waveguide Modeling Using an Iterative Finite-Difference Method with Transparent Boundary Conditions. *Journal of Lightwave Technology*. vol. 12, no. 3, pp. 465-469, 1995.

[9] W. P. Huang, C. L. Xu, S T. Chu, and S.K. Chaudhuri. The Finite Difference Vector Beam Propagation Method: Analysis and Assessment. *Journal of Lightwave Technology*. vol 10, no. 3, pp. 295-305, 1992.

[10] C. M. M. Denisse, K.Z. Troost, F. H. P. M. Habraken, W. F. van der Weg, and M. Hendriks. Annealing of plasma silicon oxynitride films. *Journal of Applied Physics*. Vol. 60, no. 7, pp. 2543-2547, 1986.

[11] René M. de Ridder, Kerstin Wörhoff, Alfred Driessen, Paul V. Lambeck, and Hans Albers. Silicon Oxynitride Planar Waveguiding Structures for Application in Optical Communication. *IEEE Jounral of Selected Topics in Quantum Electronics*. vol. 4, no. 6, pp. 930-937, 1998.

[12] K. Wörhoff, A. Driessen, P.V. Lambeck, L.T.H. Hilderink, P.W.C. Linders, Th.J.A. Popma. Plasma enhanced chemical vapor deposition silicon oxynitride optimized for application in integrated optics. *Sensors and Actuators*. Elsevier Science, vol. 74, pp. 9-12, 1999.

[13] Christophe Gorecki. Optimization of plasma-deposited silicon oxynitride films for optical channel waveguides. *Optics and Lasers in Engineering*. Elsevier Science, vol. 33, pp 15-20, 2000.

[14] R. Germann, H. W. M. Salemink, R. Beyeler, G. L. Bona, F. Horst, I. Massarek, and B. J. Offrein. Silicon Oxynitride Layers for Optical Waveguide Applications. *Journal of the Electrochemical Society*. vol. 147, no. 6, pp. 2237-2241, 2000.

[15] A. del Prado, I. Mártil, M. Fernández, G. González-Díaz. Full composition range silicon oxynitride films deposited by ECR-PECVD at room temperature. *Thin Solid Films*. Elsevier Science, vol. 343-344, pp. 437-440, 1999.

[16] John L. Vossen and Werner Kern. *Thin Film Processes II*. Academic Press, San Diego, CA, 1991.

[17] Novellus Systems User's Guide to 200 mm PECVD Processing. Novellus, 1992.

[18] Metricon User's Manual. Metricon, 2002.

[19] Thomas E. Murphy. *Integrated Optical Grating-Based Matched Filters for Fiber-Optic Communications*. Masters Thesis, MIT.

[20] Donald J. Sterling, Jr. *Technician's Guide to Fiber Optics, Second Edition*. Delmar Publishers, Albany, NY, 1993.

[21] Hermann A. Haus *Waves and Fields in Optoelectronics*. Prentice-Hall, Englewood Cliffs, NJ, 1984.

[22] Henry I. Smith. *Submicron- and Nanometer-Structures Technology*. NanoStructures Press, Sudbury, MA, 1994.

[23] Michael E. Walsh. *Nanostructuring Magnetic Thin Films Using Interference Lithography*. Masters Thesis, MIT.

[24] H. A. Haus, W. P. Huang, S. Kawakami, and N. A. Whitaker. Coupled Mode Theory of Optical Waveguides. *Journal of Lightwave Technology*, vol. LT-5, no. 1, pp. 16-23, 1987.

[25] Herman A. Haus and Weiping Huang. Coupled-Mode Theory. *Proceedings of the IEEE*, vol. 79, no. 10, pp. 1505-1518, 1991.

[26] B.E. Little and T.E. Murphy. Design Rules for Maxmally Flat Wavelength-Insensitive Optical power Dividers Using Mach-Zehnder Structures. *IEEE Photonics Letters*, vol. 9, no. 12, pp. 1607-1609, 1997.

[27] Mordehai Heiblum. Analysis of Curved Optical Waveguides by Conformal Transformation. *IEEE Journal of Quantum Electronics*, vol. QE-11, no. 2, 1975.

[28] D. Marcuse. Bending Losses of the Asymmetric Slab Waveguide. *The Bell System Technical Journal*. vol. 50, no. 8, 1971.

[29] Kwang-Ho Kwon, Seung-Youl Kang, Sang-Ho Park, Hee-Kyung Sung, Dong-Keun Kim, and Jong-Ha Moon. Additive oxygen effects in Cl_2 plasma etching of chrome films. *Journal of Materials Science Letters*, vol. 18, pp. 1197-1200, 1999.

[30] Ellen Meeks, Richard S. Larson, Pauline Ho and Christopher Apblett, Sang M. Han, Erick Edelberg, and Eray S. Aydil. Modeling of SiO_2 deposition in high density plasma reactors and comparisons of model predictions with experimental measurements. *Journal of Vacuum Science and Technology A*. vol. 16, issue 2, pp. 544-563, 1998.

[31] O.A. Popov and H. Waldron. Electron cyclotron resonance plasma stream source for plasma enhanced chemical vapor deposition. *Journal of Vacuum Science and Technology A*. vol. 7, no. 3, 1989.

[32] Katsuyuki Machida and Hideo Oikawa. SiO_2 planarization technology with biasing and electron cyclotron resonance plasma deposition for submicron interconnections. *Journal of Vacuum Science and Technology B*. vol. 4, no. 4, 1986.